



ELSEVIER

doi:10.1016/j.gca.2004.08.004

Observations of Li isotopic variations in the Trinity Ophiolite: Evidence for isotopic fractionation by diffusion during mantle melting

CRAIG C. LUNDSTROM,^{1,*} MARC CHAUSSIDON,² ALBERT T. HSUI,¹ PETER KELEMEN,³ and MARK ZIMMERMAN⁴¹Department of Geology, University of Illinois–Urbana Champaign, Urbana, IL 61801, USA²CPRG-CNRS, 54501 Vandoeuvre-lès-Nancy, France³Department of Marine Geology, Woods Hole Oceanographic Institution, Woods Hole, MA 02543, USA⁴Department of Geology and Geophysics, University of Minnesota, Minneapolis, MN 55455, USA

(Received February 19, 2004; accepted in revised form August 11, 2004)

Abstract—The Trinity peridotite (northern CA) contains numerous lithologic sequences consisting of dunite to harzburgite to spinel lherzolite to plagioclase lherzolite. Previous workers have documented geochemical gradients in these sequences consistent with melt-rock reaction processes occurring around dunites, interpreted to reflect conduits for melt ascent. We have undertaken a study of Li isotope compositions of clinopyroxene and some olivine within these sequences using ion probe techniques to test the hypothesis that the geochemical gradients are related to diffusive fluxing of alkali elements into or away from the melt conduit.

Results show large variations in $^7\text{Li}/^6\text{Li}$ occurring in a consistent pattern across three transects from dunite to plagioclase lherzolite within the Trinity peridotite. Specifically, measurements of average $\delta^7\text{Li}$ for single thin sections along the traverse reveal a low in $\delta^7\text{Li}$ in the harzburgite adjacent to the dunite returning to higher values farther from the dunite with a typical offset of ~ 10 per mil in the low $\delta^7\text{Li}$ trough. This pattern is consistent with a process whereby Li isotopes are fractionated during diffusion through a melt either from the dunite conduit to the surrounding peridotite, or from the surrounding peridotite into the dunite conduit. The patterns in $^7\text{Li}/^6\text{Li}$ occur over a length scale similar to the decrease in REE concentration in these same samples. Explaining both the trace element and Li isotopic gradients requires a combined process of alkali diffusion and melt extraction.

We develop a numerical model and examine several scenarios of the combined diffusion-extraction process. Using experimentally constrained values for the change in Li diffusion coefficient with isotope mass, large changes in $\delta^7\text{Li}$ as a function of distance can be created in year to decade timescales. The addition of the melt extraction term allows larger Li concentration gradients to be developed and thus produces larger isotopic fractionations than diffusion only models. The extraction aspect of the model can also account for the observed decrease in rare earth element concentrations across the transects. Copyright © 2005 Elsevier Ltd

1. INTRODUCTION

The importance of reactions between ascending melts and mantle in affecting both the physics of magma ascent in the mantle (Aharonov et al., 1997; Kelemen et al., 1997; Spiegelman et al., 2001) and the geochemical signatures of erupted lavas (Navon and Stolper, 1987; Asimow et al., 1999; Lundstrom, 2000a; Jull et al., 2002) is increasingly realized. Geochemical evidence suggests that ascending melts beneath midocean ridges are channelized in dunites created by melt-rock reactions (Kelemen et al., 1995, 1997, 2000). Because of channelization, ascending melts do not directly react with the peridotite surrounding the melt conduit, resulting in orthopyroxene undersaturation in MORB (O'Hara, 1968; Stolper, 1980) and highly depleted trace element concentrations in abyssal peridotites (Johnson et al., 1990; Dick and Natland, 1996). However, ascending, channelized melts could affect melting in the surrounding peridotite if alkali elements diffuse away from the conduit into the surrounding peridotite (Lundstrom, 2000b). Laboratory experiments demonstrate that alkali elements, particularly sodium, will rapidly diffuse from an alkali basalt into the interstitial melt within peridotite at low pressure, causing orthopyroxene to preferentially dissolve

(Lundstrom, 2000b, 2003). Because the effect of increasing bulk sodium content on melt-peridotite equilibria dramatically increases at lower pressures (Kushiro, 1975; Hirschmann et al., 1998), this process could have fundamental importance to the overall production of the oceanic crust. However, the hypothesis that sodium diffusively fluxes the peridotite surrounding a melt conduit, based solely on laboratory experiments, has little observational evidence supporting its occurrence.

Lithium, an alkali element of smaller ionic radius than sodium, is known to diffuse extremely rapidly. Recent experiments have demonstrated that Li isotopes are fractionated during diffusion through silicate melts (Richter et al., 2003); thus Li isotopes should serve as an indicator of the alkali diffusive fluxing process. Here, we test the hypothesis that melt-rock reactions related to alkali diffusion occur adjacent to mantle melt conduits through measurement of Li isotopes in lithologic transects in the Trinity Ophiolite. Our results show that the Li isotopic compositions of samples vary in a systematic pattern across three transects, consistent with alkalis diffusing through interconnected melt within the different lithologies.

2. USING Li ISOTOPES TO IDENTIFY ALKALI DIFFUSION PROCESSES

Lithium is an element under increasing geochemical scrutiny due to rapid advances in analytical techniques and interest in

* Author to whom correspondence should be addressed (lundstro@uiuc.edu).

light element geochemistry. Current understanding of Li isotope geochemistry, particularly with respect to processes at high temperature, remains incomplete. Li concentrations in basalts vary between 4 and 10 $\mu\text{g/g}$ and the Li concentration of average NMORB is 4.3 $\mu\text{g/g}$ (Sun and McDonough, 1989). Based on comparison to other elements in mantle-derived basalts, Ryan and Langmuir (1987) infer that Li behaves with an incompatibility similar to that of Yb. Li has two isotopes (^6Li and ^7Li) that differ in mass by 16% and significant variations in $^7\text{Li}/^6\text{Li}$ occur at the per mil level in earth materials (Chan et al., 1988, 1992). The ^7Li to ^6Li ratio is reported relative to a standard using the delta notation with $\delta^7\text{Li} = [(^7\text{Li}/^6\text{Li})_{\text{sample}} / (^7\text{Li}/^6\text{Li})_{\text{L-SVEC-1}}] \times 1000$ where L-SVEC is a lithium carbonate standard. Although the terrestrial mass balance for Li isotopes remains to be established, $\delta^7\text{Li}$ for mantle derived basalts generally ranges from +3 to +6, seawater has a $\delta^7\text{Li}$ of +32 and sediments and other upper crustal rocks generally fall between these values (Tomascak, 2004). However, continental crust samples appear to have lower $\delta^7\text{Li}$ than the mantle value of +3 to +6 (Teng et al., 2004). The lithium isotopic composition of carbonaceous chondrites also remains to be established but the few measurements to date indicate that $\delta^7\text{Li}$ appears to be similar to that of terrestrial mantle basalts (James and Palmer, 2000; McDonough et al., 2003).

Although equilibrium fractionation of light element isotopes based on differences in bond energies is significant in low temperature processes, equilibrium isotopic fractionations are very small at higher temperatures. Although this has not yet been experimentally verified for Li, an analysis of several volcanic rocks from Hawaii related by crystal fractionation found no change in $^7\text{Li}/^6\text{Li}$ (Tomascak et al., 1999). If bonding during high temperature processes does not shift Li isotope ratios, are there any other high temperature processes that can fractionate Li isotopes? If there are not, crustal recycling and input of Li fractionated by low temperature processes at subduction zones would represent the only process creating the Li isotope heterogeneity observed in the mantle. Indeed, most studies of Li isotopes in mantle and mantle-derived magmas to date have assumed there are no processes fractionating Li isotopes within the mantle. However, kinetic fractionation of isotopes can occur during the high temperature process of diffusion (e.g., Richter et al., 1999, 2003).

Alkali elements are known to diffuse through silicate melts more than an order of magnitude faster than other elements at magmatic temperatures (Mungall, 2002). The diffusivity of alkalis in silicate melts increases with decreasing ionic radii; a minimum estimate for the Li effective binary diffusion coefficient in a basanite-tholeiite melt diffusion couple at 1723 K is $6 \times 10^{-6} \text{ cm}^2/\text{s}$ (Lundstrom, 2003). Richter et al. (2003) determined the diffusivity of Li in basalt at 1623 K to be $7 \times 10^{-5} \text{ cm}^2/\text{s}$, almost two orders of magnitude higher than any other element in their basalt-rhyolite diffusion experiment. Thus, lithium is one of the fastest diffusing elements in silicate melts.

Lithium is a mildly incompatible element within the mantle (Brenan et al., 1998) such that in a polybaric melting column, Li concentrations in the earliest formed "deep" melts should be higher than those of later formed melts in the already depleted shallow mantle. Therefore, as melts from depth ascend through a melt conduit, a gradient of decreasing Li concentration with

distance away from the conduit should in principle exist to drive Li diffusion from the conduit into the surrounding harzburgite or lherzolite. However, dunites are generally observed to have lower concentrations of incompatible elements than surrounding harzburgite and lherzolite which could cause Li to diffuse through a melt toward the dunite.

Because of the large relative mass difference, lithium isotopes should be fractionated during diffusion. While the ratio of diffusion coefficients between two ideal gases with different masses is inversely proportional to the ratio of the masses raised to the 0.5 power, this exponent, expressed as β (Richter et al., 1999), is much less than 0.5 in condensed matter. Experiments examining isotopic shifts during diffusion in silicate melts gave values for β of 0.1 for Ca and <0.05 for Ge, respectively (Richter et al., 1999), while very recent work determined a β of ~ 0.215 for Li (Richter et al., 2003). This value of β means that $D_{^6\text{Li}}$ is 1.035 times greater than $D_{^7\text{Li}}$ resulting in magmatic processes being able to create large Li isotope fractionations by diffusion.

Lithium could therefore provide an ideal tool for assessing the role of flux melting by alkali diffusion during melting. If Li diffuses from ascending melt within a dunite conduit into the intergranular melt in the surrounding peridotite, Li isotopic fractionation should occur. These isotopic shifts will be recorded in the peridotite minerals if equilibration between melt and minerals is fast (i.e., occurs by dissolution and reprecipitation rather than solid state diffusion). As an example, Figure 1 shows a diffusion-couple model using constant initial $^7\text{Li}/^6\text{Li}$, diffusion driven by a factor of ten difference in concentration, and diffusion coefficients that differ by 3.5%; this results in a trough of low $\delta^7\text{Li}$ on the low concentration side of the couple with more than a 23% offset in $\delta^7\text{Li}$. In this model, the amplitude of the trough is controlled by β and the initial ratio of the concentrations driving the diffusion while the width of the trough and distance that the trough has migrated reflects the time over which the process has occurred (Richter et al., 1999). Thus, if diffusion of Li occurred analogously to other alkalis during melt ascent, relatively large variations in $\delta^7\text{Li}$, resolvable by modern in situ isotopic methods, should be readily observable.

3. GEOLOGIC SETTING AND SAMPLES

The Trinity peridotite is an ultramafic body located in the eastern Klamath Mountains of northern California. Ultramafic rocks occur over an area ~ 50 km wide by 75 km long and are interpreted to represent an ophiolite reflecting a former spreading center within a back arc or marginal basin setting (Quick, 1981a). There remains some uncertainty regarding the geochronology of events in the Trinity peridotite but the range of dates probably indicates a polygenetic history. Based on ages of plagiogranites that intrude the gabbros of the ophiolite and structural relations to these bodies, plastic deformation in the peridotite body is interpreted to have ceased by 450–480 Ma (Lanphere et al., 1968; Quick, 1981a). A single two point Sm-Nd isochron indicates an age of 472 ± 37 Ma for the plagioclase lherzolite at China Mountain (Jacobsen et al., 1984). A whole rock Sm-Nd array from Toad Lake produced an age of 423 ± 48 Ma, leading to the conclusion of Gruau et al. (1991) that the Trinity complex as whole except China Moun-

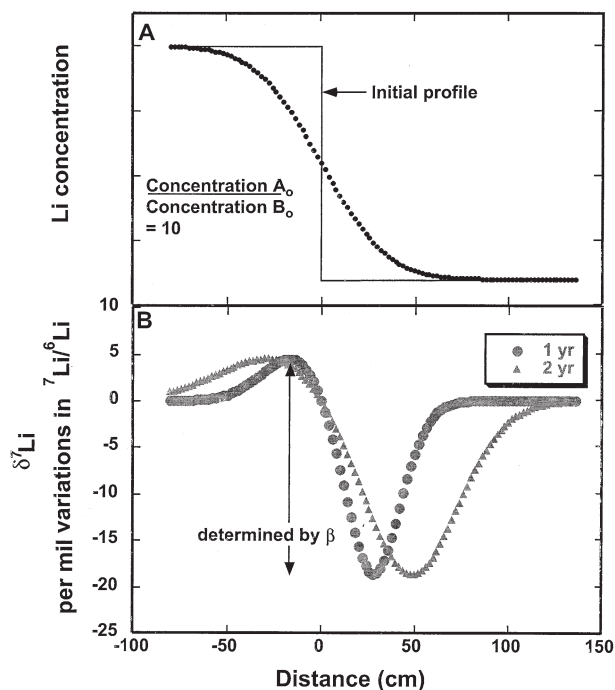


Fig. 1. Calculated change in Li concentration (A) and $\delta^7\text{Li}$ (B) as a function of distance for a model of a melt-melt diffusion couple with an initial ratio in Li concentrations of 10. The relative diffusion rates of ^6Li and ^7Li and thus isotopic fractionation are determined by β (see text), which is experimentally constrained to be 0.215, and the initial concentration ratio (Richter et al., 2003). This model predicts a 23‰ change in $\delta^7\text{Li}$. The position of this trough will progressively move with time; here a value of $6 \times 10^{-6} \text{ cm}^2/\text{s}$ for ^7Li is used, resulting in the trough migrating 50 cm into the peridotite in 2 yr time.

tain are part of a cogenetic igneous suite of age 420–440 Ma. Furthermore, these studies, along with Gruau et al. (1995), indicate that there is considerable variation in ϵNd (T) and $^{87}\text{Sr}/^{86}\text{Sr}$ within the Trinity ophiolite. Indeed, within a single 20 m long outcrop, Gruau et al. (1995) document two lherzolite samples differing by 7 ϵNd units and a gabbroic dyke, also of distinct ϵNd .

The Trinity peridotite, like many ultramafic bodies globally, contains numerous lithologic sequences of dunite-harzburgite-spinel lherzolite-plagioclase lherzolite that occur over centimeters to hundreds of meters length scales. These sequences have been interpreted to be reaction zones around conduits of ascending melt (Quick, 1981a,b; Kelemen et al., 1992). Quick (1981a) observed systematic changes in the major element composition of mineral phases as a function of distance from a dunite and first proposed that the dunite reflected reaction between an ascending basaltic melt and the host peridotite (assumed to be plagioclase lherzolite). Kelemen et al. (1992) analyzed clinopyroxenes within some of the same samples as Quick (1981a) by secondary ion mass spectrometry (SIMS) and found a systematic increase in rare earth element concentration (REE) as a function of distance away from dunite. This was interpreted to reflect lateral advection of melt out from the dunite causing clinopyroxene to be dissolved out of the original plagioclase lherzolite producing harzburgite.

The question of the timing of dunite formation may impact assumptions regarding the initial alkali concentration gradients

driving diffusion between dunite and surrounding lherzolite. The structural relationship of Trinity dunites cross-cutting the peridotite foliation indicates that the dunites probably formed after corner flow deformation of the host peridotites had ceased (Quick, 1981a); however, laboratory experiments indicate that melt conduits at high angle to the foliation could also result from shear during corner flow (Holtzman et al., 2003) so that the simple model of polybaric asthenospheric melting where Li concentrations may have been greater in the dunite cannot be ruled out. An important point is that plagioclase lherzolite in the Trinity is very fertile, with clinopyroxene heavy REE_(N) (chondrite normalized abundance) of 15–20 while clinopyroxenes in the dunites have lower heavy REE_(N) of 3–5 (Kelemen et al., 1992). Based solely on its similar incompatibility to HREE, Li might be expected to have a similar concentration gradient as the HREE such that Li diffusion could have been driven from the lherzolite into the dunite.

Samples for this study come from three dunite to plagioclase lherzolite transects ranging over two orders of magnitude in length. Samples were either thin sections prepared from hand specimen or 1 inch (2.54 cm) diameter drill core. Olivine and orthopyroxene grain sizes generally range from 1 to 3 mm in size while clinopyroxenes are typically smaller (Quick, 1981b). Transect TP90-9 consists of a dunite to harzburgite to spinel lherzolite to plagioclase lherzolite sequence of ~ 200 cm length collected from Vicki Bluff (studied previously by Kelemen et al., 1992). Transect TP90-20 also consists of a dunite to plagioclase lherzolite transect of ~ 2000 cm length located on Vicki Bluff. Finally, transect VB91 reflects a 20 cm sequence of dunite to plagioclase lherzolite, taken as drill cores oriented parallel to the observed dunite/harzburgite contact located on the southeast exposure of Vicki Bluff.

All of the rocks have undergone varying degrees of serpentinization. Olivines are the most altered resulting in the dunites having the highest degree of serpentinization. Quick (1981a) estimated that 20%–50% of the individual rock types in the Trinity are serpentinized. Clinopyroxenes and orthopyroxenes are much less altered such that they stand out above the serpentine matrix in many thin sections.

4. METHODS

4.1. Li Isotope Analysis

Lithium isotope ratios were measured on clinopyroxenes and olivines by SIMS on a Cameca IMS-1270 and a Cameca IMS-3f, both located at CRPG-CNRS Nancy, France, using established techniques (Chaussidon and Robert, 1998; DeCitre et al., 2002; Beck et al., 2004). Mineral grains in the diffusion-reaction experiment were analyzed using the Cameca IMS-5f at the Center for Microanalysis of Materials at the University of Illinois (using the same analytical conditions as for the Nancy IMS-3f). A 10 kV (for the IMS-3f) and 12.5 kV (for the IMS-1270) negative oxygen primary beam ranging in intensity between 20 and 60 nA and in size between 25 and 40 μm diameter was used for sputtering. Positive secondary Li ions were extracted with an accelerating voltage of 4.5 kV (IMS-3f or -5f) or 10 kV (IMS-1270). Mass resolution was set at ~ 1500 for the two instruments and no energy filtering was used for the Li isotope analysis, the energy slit being centered and fully opened. Li isotopes were measured using the electron multiplier by peak hopping between mass 6 and 7 with internal (counting statistics based) 1σ standard errors ranging from less than 1‰ to a few per mil. Count rates for ^6Li in the lowest concentration samples remained greater than 100 cps. Instrumental mass discrimination during Li analysis, the offset between the measured ratios and “true” values, is significant and of opposite sense to that observed for

Table 1. Compositions of CPX standards.

	BZ226	BZ.CG
SiO ₂	51.36	50.35
Al ₂ O ₃	4.49	7.05
FeO	3.63	2.96
MgO	15.35	14.11
CaO	22.23	21.71
Na ₂ O	0.81	1.32
K ₂ O	0.005	0.008
TiO ₂	0.26	0.37
$\delta^7\text{Li}$	-4.1	10.5
2 σ (per mil)	1	1

other isotopic systems. The reported $\delta^7\text{Li}$ values have been corrected for this offset using a set of two clinopyroxene standards (CPX BZ 226 and CPX BZ.CG) and an olivine standard (OL BZ 29) previously analyzed for $^7\text{Li}/^6\text{Li}$ ratio by thermal ionization mass spectrometry (TIMS) and checked for isotopic homogeneity by SIMS (DeCitre et al., 2002). Repeated analyses of these standards with the IMS-3f (Beck et al., 2004) has shown that (i) the instrumental mass discrimination was stable within $\pm 1.5\%$ ($\pm 1\sigma$) for a given mineral, (ii) that the matrix effects on instrumental mass discrimination between different minerals were less than $\pm 1.5\%$ and (iii) that this instrumental mass discrimination was stable within $+ 1.5\%$ over a the 15% isotopic variation range of the standards. The compositions of the two clinopyroxene

standards are given in Table 1 and can be compared with measured clinopyroxene compositions in thin sections from transect VB-91 (Table 2). A total uncertainty of $\pm 2.2\%$ ($\pm 1\sigma$) can be assumed for all the present measurements, unless specified differently (Table 3). A subset of these samples was also analyzed for B concentrations and B isotopes using previously reported procedures (Chaussidon and Marty, 1995). $\delta^{11}\text{B}$ values are reported relative to NBS 951 with an average uncertainty of $\pm 2\%$ (1σ).

Each thin section sample was measured in at least 2 and generally 4–8 analytical points with the exception of one sample that was measured in greater than 50 analytical spots. Analyses occurred on at least 2 different clinopyroxenes within each sample. For most samples, the uncertainties in individual measurements (internal precision) are much smaller than the variation in spot to spot measurements (external precision) of grains within the same thin section. Therefore, the errors reported in Table 3 reflect the standard deviation (1σ) of the spot to spot (usually grain to grain) variation within a single thin section. Because of a much larger variability of $\delta^7\text{Li}$ found initially in sample TP90-20-2 (a dunite), this sample was analyzed in much greater detail to better understand the origin of the $\delta^7\text{Li}$ variability. Li and B concentrations for transects TP90-20-2 and VB-91 reported in Table 3 are based on the ratio of the count rate to the primary beam current for the sample relative to that for standards during the same analytical session. This procedure is more rapid but less precise than the classical technique of energy filtering of intensity ratios to Si, but comparisons between the two approaches have shown that relative concentration variations can be determined with an uncertainty of $\pm 20\%$. Li concentrations in transect TP90-9 were analyzed by measuring Li/Si in the

Table 2. EDS analyses.^a

	Dunite VB91-34		Harzburgite VB91-36		Spinel Lherzolite VB91-39		Iherzolite 9030 ^b
Olivine							
SiO ₂	41.33	0.05	41.17	0.09	41.06	0.07	40.76
FeO	9.92	0.06	9.73	0.16	9.69	0.12	9.32
MgO	48.74	0.09	49.11	0.07	49.26	0.17	49.37
Mg#	89.8		90.0		90.1		90.5
Spinel							
TiO ₂	0.25	0.03	0.09	0.00	0.13	0.04	0.25
Al ₂ O ₃	28.19	0.06	31.04	0.33	31.26	0.31	33.09
FeO	21.29	0.73	17.94	0.21	18.06	0.23	16.03
MgO	11.65	0.13	13.04	0.06	12.82	0.00	15.34
Cr ₂ O ₃	38.63	0.51	37.90	0.49	37.74	0.11	33.94
Mg#	52.3		57.6		56.6		
Cr#	47.9		45.0		44.7		
Clinopyroxene							
SiO ₂	52.04	0.19	51.96	0.08	51.92	0.03	51.65
Al ₂ O ₃	3.70	0.21	3.71	0.21	3.66	0.07	3.55
TiO ₂	0.26	0.02	0.21	0.03	0.24	0.03	0.3
Cr ₂ O ₃	1.13	0.07	1.29	0.08	1.26	0.15	1.06
FeO	2.44	0.05	2.18	0.14	2.32	0.08	2.68
MgO	17.78	0.20	17.65	0.11	17.73	0.22	17.9
CaO	22.26	0.21	22.65	0.44	22.51	0.16	22.31
Na ₂ O	0.38	0.04	0.37	0.01	0.37	0.01	0.26
Mg#	92.9		93.5		93.2		92.3
Orthopyroxene							
SiO ₂			55.59	0.08	55.43	0.12	55.68
Al ₂ O ₃			2.56	0.08	2.54	0.06	3.44
Cr ₂ O ₃			0.72	0.00	0.66	0.04	0.53
TiO ₂			0.13	0.01	0.16	0.01	0.1
FeO			5.81	0.01	5.89	0.04	6.26
MgO			34.17	0.02	34.45	0.09	33.2
CaO			1.04	0.01	0.87	0.17	0.54
Mg#			91.3		91.2		90.5

^a EDS analyses using the JEOL840A SEM in the Department of Geology, UIUC, using the following conditions and standards: 15 kV, 10 nA, San Carlos olivine, diopside glass, Kakanui hornblende, Cr₂O₃, rutile and anorthite glass. Errors reflect 1 σ variation on 3–4 analyses.

^b Quick (1981).

Table 3. Ion probe analyses of Li and B in clinopyroxene.

Sample	n	Distance ^a	$\delta^7\text{Li}$	Error ^b	Li (ppm)	Error ^b	$\delta^{11}\text{B}$	Error ^b	B ppm	Error ^b
TP90-20 transect										
TP90-20-2 (Mar. 2002) ^c	48	-73.8	14.3	10.0	1.9	2.0				
TP90-20-2 (Sept. 2002) ^c	6	-73.8	10.6	11.2	0.9	0.4	-12.0	4.0	0.11	0.07
TP90-20-4	5	16.2	2.3	1.4	2.4	1.1				
TP90-20-7	2	144.2	2.5	3.1	1.0	0.2	-19.1	5.6	0.20	0.05
TP90-20-9	3	243.0	1.6							
TP90-20-12	2	462.7	12.5	2.2	1.6	0.1	-16.3	5.0	0.6	0.4
TP90-20-13	7	522.1	8.7	1.8	1.6	0.6				
TP90-20-19	8	1602.8	12.1	1.1	2.4	0.4	-14.8	0.5	0.4	0.3
VB91 transect										
VB91-34	8	0.0	6.0	2.1	2.0	0.4				
VB91-35	3	2.9	3.3	3.2	4.9	1.3				
VB91-36	9	5.7	-1.5	3.3	3.7	1.3				
VB91-38	3	11.2	5.1	2.8	8.5	1.4				
VB91-40	4	16.5	3.7	2.4	2.9	0.6				
TP90-9 transect										
TP90-9-14	7	-12.9	2.8	2.0	1.6	0.4				
TP90-9-12	2	-11.7	5.0	2.4	2.1	0.0				
TP90-9-3	8	-3.4	-1.4	2.5	2.5	1.2				
TP90-9-4a	7	8.0	0.2	2.5	2.6	0.6				
TP90-9-5	4	13.6	-5.8	1.0	2.7	0.2				
TP90-9-6	6	29.9	-1.1	4.2	2.5	0.7				
TP90-9-7	6	53.3	-1.8	2.2	2.4	1.1				
TP90-9-8	4	77.2	-1.2	3.4	1.8	0.3				
TP90-9-9	5	123.6	5.0	1.7	2.9	0.8				
TP90-9-10b	6	165.2	4.9	1.1	2.6	0.9				
TP90-9-11b	11	201.1	11.2	3.5	1.5	0.2				

Note: Individual analyses making up these average can be obtained at the GCA electronic annex (EAI), n refers to number of Li analyses; some B averages reflect fewer data (see annex).

^a Reflects measured distance in cm from harzburgite-dunite contact.

^b Errors given reflect 1 σ variation on the population (n) of ion probe analyses for a sample.

^c Date reflects time of analytical session.

same analytical spots as the isotopic analysis and correcting for useful yields based on a concentration standard analyzed in the same session.

4.2. Elemental and Imaging Analysis

Digital imaging was used to determine the modal abundance of minerals in samples from transect VB91 using back scattered electron images collected with the JEOL 840A SEM located in the Department of Geology at UIUC. Mg X-ray maps were collected simultaneously and used to distinguish olivine, orthopyroxene, spinel and clinopyroxene. The total number of pixels covered by each phase within >8 separate BSE images (2.5 mm²) was summed and converted into modes directly based on percentage area covered. No compensation for phase volume changes with serpentinization was applied. To assess the accuracy of this mode counting technique, we produced a synthetic peridotite "standard" by pressing weighed out mineral separates of grain size similar to our samples in a piston cylinder apparatus at 1 GPa and 1000°C. The resulting charge was sliced and mounted to produce an area of peridotite similar to that from a 2.54 cm diameter core. The modal percentages by digital image analysis were 59% olivine, 25% orthopyroxene, and 16% combined clinopyroxene-spinel compared to the values of 61% olivine, 25.5% orthopyroxene, and 13.4% clinopyroxene-spinel, based on the weighed-in amounts.

Individual mineral compositions for transect VB91 reported in Table 2 were determined by energy dispersive X-ray spectroscopy (EDS) using a 4Pi analysis system on the JEOL 840A. Natural mineral standards were used and oxide abundances were calculated using corrections for atomic number, absorption and fluorescence (ZAF). Analysis conditions were 15 kV accelerating voltage and 10 nA current with a beam size of ~3 μm . Analysis of Na and K across transects VB91 and TP90-9 was performed on the Cameca IMS 5f using a O-beam of 20 nA and an energy filtering of 50 V offset and window of ± 19 eV. Concentration were calculated based on analysis of Smithso-

nian standard Arenal Hornblende under the same conditions. Each point represents the average of 3 ion probe analyses within 1–2 different clinopyroxene in each sample. The major objective of these analyses was to document variations across the transect; accuracy is estimated at $\pm 20\%$ relative.

4.3. Experimental Approach to Li Isotopic Fractionation

We performed a laboratory experiment to simulate Li diffusion through a partially molten peridotite. Although the experiments of Richter et al. (2003) provide critical constraints on the Li isotope diffusion coefficients and β , it is not known whether mantle minerals will behave as reactive or passive solids during a diffusive infiltration process within the mantle. With this in mind, we performed a two-stage piston cylinder experiment similar to experiments described in Lundstrom (2003). The diffusion couple consisted of a basanite (EL-10 from the Canary Islands) doped with an enriched ⁶Li tracer (~1000 $\mu\text{g/g}$) and a partially molten harzburgite containing ~10% alkali rich melt (~5 wt% Na₂O, 5 wt% K₂O and ~250 $\mu\text{g/g}$ Li with ⁷Li/⁶Li of ~4). Thus, the purpose of the experiment was not to determine β but rather trace changes in ⁷Li/⁶Li in the minerals as the melt ⁷Li/⁶Li changed. The two halves of the experiment were synthesized (or hot pressed) in the piston cylinder for 42 h at 0.9 GPa pressure and 1523 K. After polishing the faces of the sections to be joined, the two materials were juxtaposed at the same pressure and temperature as the hot press condition for 7 min. As detailed in Lundstrom (2003), temperature variations through the diffusion couple were <10°C. The resulting charge was sectioned, polished and analyzed for major elements using SEM-EDS and for Li isotopes using the ion probe. Ion probe analyses were performed in the basanite melt, in the glass pockets within the harzburgite and within the largest mineral grains in each half of the couple.

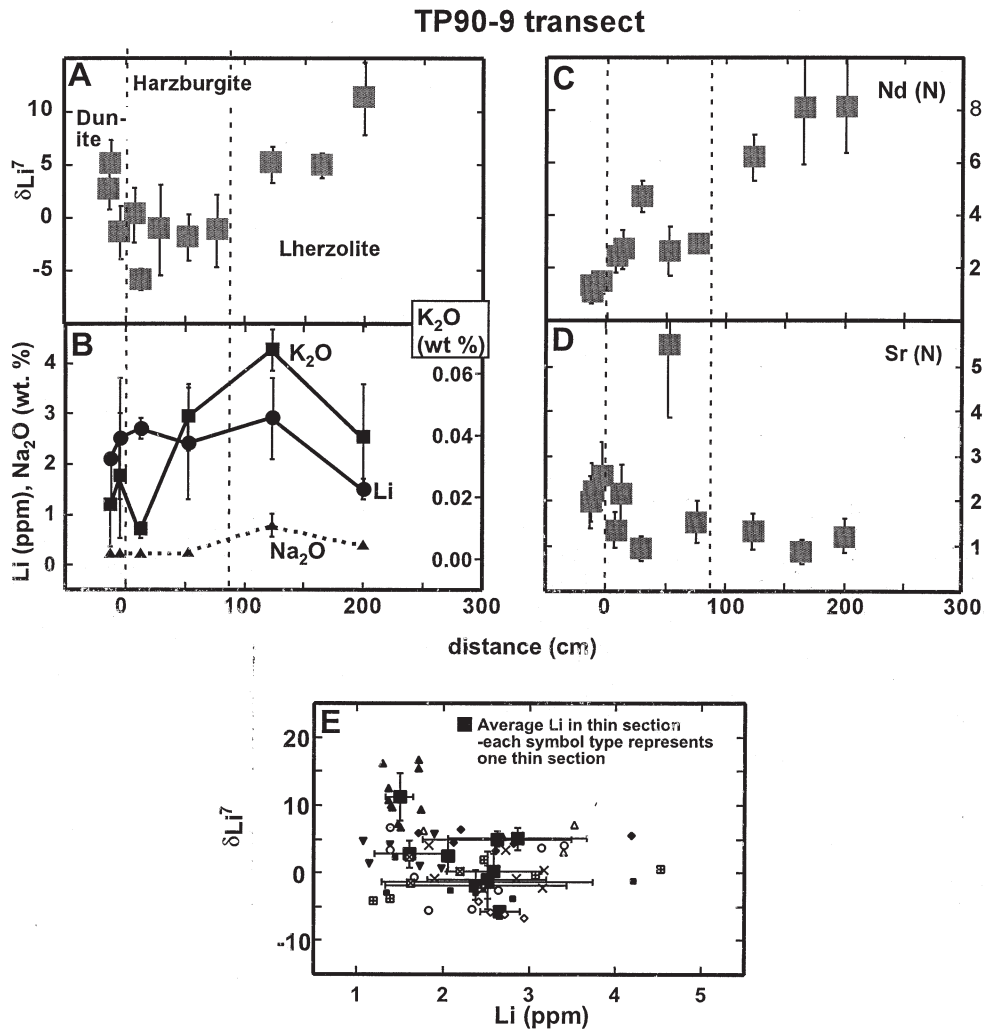


Fig. 2. Average $\delta^7\text{Li}$, Na, Li, K and Nd and Sr contents of clinopyroxenes in single thin sections from samples from transect TP90-9 as a function of distance from the dunite-harzburgite boundary. A) $\delta^7\text{Li}$ decreases in the harzburgite immediately adjacent to the dunite and then increases again farther into the peridotite. B) Alkali element concentrations show no systematic change across the transect. This behavior contrasts with Nd and other REE; C) Over the same length scale, Nd concentrations decrease approaching the dunite (data from Kelemen et al., 1992). Since the Li diffusion coefficient is at least $60\times$ greater than that of Nd (Lundstrom, 2003; Richter et al., 2003), the process creating these combined profiles cannot reflect diffusion alone. D) Most incompatible element concentrations behave like Nd but not all. Sr concentrations, for instance, remain constant and then increase slightly near the dunite-harzburgite boundary. E) Li concentration vs. $\delta^7\text{Li}$ for individual analyses and for thin section averages. Unlike sample TP90-20.2, no trend in Li concentration vs. $\delta^7\text{Li}$ is seen for any individual thin section. Excluding sample (TP90-9.11b), located farthest from the dunite and having the highest $\delta^7\text{Li}$ and lower Li concentration, there is no relationship between Li concentration and $\delta^7\text{Li}$.

5. RESULTS

5.1. Trinity Transects

Table 3 reports the average of all Li analyses for a single sample and the 1σ variation of the analysis population for that sample (individual analyses provided as electronic annex (EA); AE Table 1). Average $\delta^7\text{Li}$ for the different samples varies from -5.8 to 14.3 . The absolute external error on thin section averages is typically $1-3\%$ (1σ) with one exception (TP90-20.2). $\delta^7\text{Li}$ analyses at different locations on the same clinopyroxene grain vary beyond the measurement error (internal precision). However, the differences in $\delta^7\text{Li}$ between distinct grains are typically larger than within single grains.

In each of the three transects, there is a repeated pattern of a 5 to 10‰ decrease in the $\delta^7\text{Li}$ going from the dunite into the adjacent harzburgite followed by a rise back to higher $\delta^7\text{Li}$ farther into the peridotite. Transect TP90-9 shows this most clearly with the 5 samples found between the sharp dunite-harzburgite contact and the plagioclase-in boundary having distinctly lower $\delta^7\text{Li}$ than any of the 3 plagioclase lherzolite samples and lower than the two dunite samples (Fig. 2a). Transect VB91, 20 cm in length and having only five samples analyzed, produces the same pattern with a harzburgite sample located within 5 cm of the dunite having the lowest $\delta^7\text{Li}$ of the transect (Fig. 3). The longest transect, TP90-20, also shows the

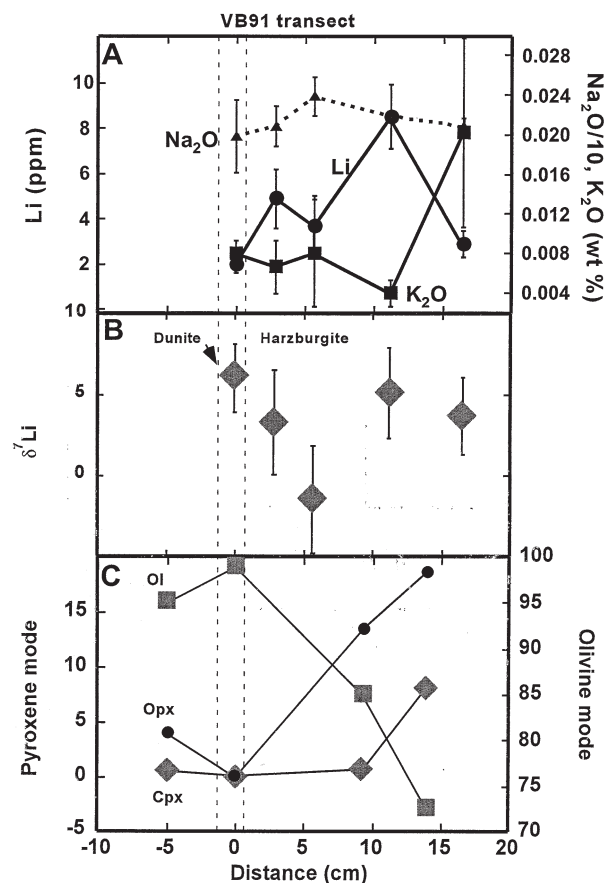


Fig. 3. A) Alkali element concentrations in clinopyroxenes, B) Average $\delta^7\text{Li}$ of clinopyroxenes and C) mineral modes for samples from transect VB91, as a function of distance from the center of a small dunite. Like transect TP90-9, $\delta^7\text{Li}$ decreases in the harzburgite immediately adjacent to the dunite and then increases again farther into the peridotite. Alkali concentrations show no systematic change across the transect.

lowest $\delta^7\text{Li}$ in samples within the harzburgite adjacent to the dunite-harzburgite contact and higher $\delta^7\text{Li}$ at greater distances from the dunite (Fig. 4). However, the sole dunite sample analyzed for this transect, TP90-20-2, shows large variation in $\delta^7\text{Li}$ resulting in no significant difference between it and the adjacent harzburgite samples.

To understand the source of the variability observed in TP90-20-2, we undertook a detailed examination of this sample through multiple analyses (>50) of clinopyroxenes and olivines (AE Table 2; data available for download at GCA Web site). Within this single sample, $\delta^7\text{Li}$ in clinopyroxene varies from ~ 7 to 38 while that in olivine ranges from -5 to 21. Li concentrations vary widely and negatively correlate with $\delta^7\text{Li}$ for olivines (Fig. 5). This correlation is present but less clear for clinopyroxenes. Notably, the trend of Li vs. $\delta^7\text{Li}$ for olivine appears to be offset from the trend for clinopyroxene with the latter having higher average $\delta^7\text{Li}$ and slightly higher Li contents than the former. The extreme $\delta^7\text{Li}$ variability in TP90-20-2 was not observed in any other sample including the dunitites from the other two transects.

Average Li concentrations within the clinopyroxenes analyzed range from 0.9 to 8.5 $\mu\text{g/g}$ with Li concentrations gen-

erally more variable than $\delta^7\text{Li}$. Like $\delta^7\text{Li}$, the greatest variability in Li concentration occurs in dunite TP90-20-2. Li concentrations within transect TP90-20 increase with distance away from the dunite whereas samples from transect VB91 and TP90-9 show no simple relation between Li concentration and distance. Ion probe analyses of Na and K also show no simple relationship with distance in either VB91 or TP90-9 (Figs. 2 and 3). Boron concentrations in clinopyroxene range between 0.06 and 0.6 $\mu\text{g/g}$ and increase with distance away from dunite in transect TP90-20. The behavior of Li and B concentrations decreasing toward the dunite in TP90-20 mimics the behavior of other incompatible elements such as the REE that have their lowest concentrations within clinopyroxenes in dunite (Kelemen et al., 1992).

The Li concentration vs. $\delta^7\text{Li}$ relationship for individual analyses within the TP90-9 transect (Fig. 2E) show a rough

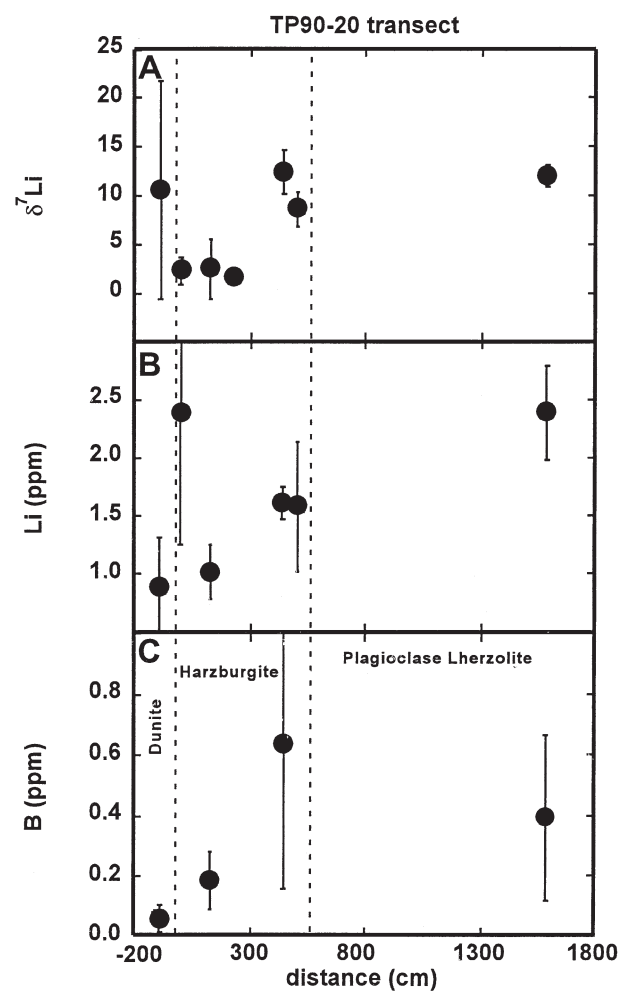


Fig. 4. Average $\delta^7\text{Li}$, Li and B contents of clinopyroxenes in single thin sections from transect TP90-20 as a function of distance from the dunite-harzburgite boundary. A) $\delta^7\text{Li}$ is lowest in the harzburgite immediately adjacent to the dunite and then increases again farther into the peridotite. The $\delta^7\text{Li}$ in the sole dunite sample from this transect (sample farthest to the left) is highly variable, reflecting variations within individual mineral grains related to Li concentration (see Fig. 5). (B, C) Li and B contents decrease approaching the dunite, similar to other incompatible elements.

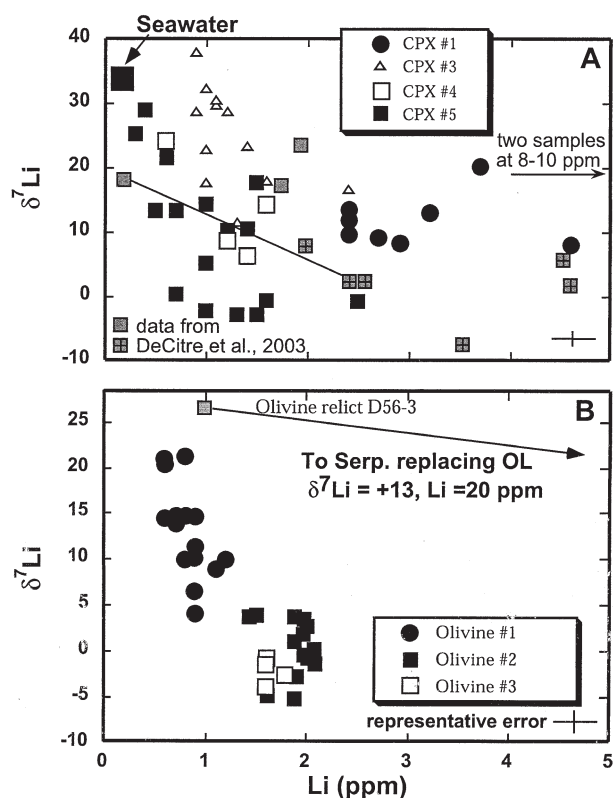


Fig. 5. $\delta^7\text{Li}$ of individual analyses in thin section TP90-20-2 as a function of Li concentration for (A) clinopyroxene and (B) olivine. Both diagrams show as common symbols analyses of individual mineral grains (with distinct numbers) within the thin section. An inverse correlation between $\delta^7\text{Li}$ and Li, more prominent for olivine than clinopyroxene, exists within individual mineral grains (individual analysis data available as AE Table 2). For reference, the position of seawater (Li concentration in seawater) and data from DeCitire et al. (2002; gray squares representing relict minerals while squares with crosses represent serpentinized minerals) are also shown. Arrows connect relict and serpentinized portion of the same mineral. The inverse correlation, along with observations from DeCitire et al. (2002), suggest that preferential leaching of ^6Li during serpentinization may have occurred in this sample. However, the slope of the observed data and the relict-serpentine pairs of DeCitire et al. (2002) are not similar. The extreme variability in $\delta^7\text{Li}$ of this sample is not observed in any other sample.

pattern broadly similar to the trend within TP90-20-2 (Fig. 5). However, none of the individual thin sections produce trends mimicking the inverse relationship observed in TP90-20-2 clinopyroxenes. Close examination of Figure 2E shows that any inverse relationship observed entirely reflects the data from TP90-9-11, the sample furthest from the dunite in the transect.

The extensive analysis of TP90-20-2 includes measurements of $\delta^{11}\text{B}$ in clinopyroxene ($n = 6$) and olivine ($n = 4$). Clinopyroxenes have an average $\delta^{11}\text{B}$ of -12 while olivines average -16 with external errors of $\sim 4\%$ each, resulting in overlapping isotopic compositions. Both of these values fall within the range of $\delta^{11}\text{B}$ found in melt inclusions from Iceland but are slightly lighter than those typically found in MORB or convergent margin magmas (Chaussidon and Marty, 1995; Gurenko and Chaussidon, 1997). The 4% external error (1σ) results from the low count rates on the B analyses with typical 1σ

counting statistics precision on analysis of 5% for clinopyroxene to 8% for olivine. B concentrations in olivine range from 10 to 56 ppb, consistent with equilibrium with a melt of 1–5 ppm B (Brenan et al., 1998); for comparison, island arc tholeiites have 3–8 ppm B (Moriguti and Nakamura, 1998). Average $\delta^{11}\text{B}$ for two other samples from the TP90-20 transect (TP90-20-7 and TP90-20-12) are -19 and -16 respectively, indicating no difference in $\delta^{11}\text{B}$ between dunite and other lithologies or any systematic pattern through the sequence.

5.2. Piston Cylinder Diffusion Experiment

$^7\text{Li}/^6\text{Li}$ of the glasses in the piston cylinder experiment smoothly varies between the end member compositions (Fig. 6). Notably, the profile does not occur symmetrically across the original interface (denoted by the suture of the capsule halves) but rather the major changes in $^7\text{Li}/^6\text{Li}$ occur entirely within the harzburgite portion of the experiment. The $^7\text{Li}/^6\text{Li}$ of the basanite is higher than that of the starting basanite indicating preferential loss of ^6Li to the harzburgite half of the experiment. The flat profile of $^7\text{Li}/^6\text{Li}$ in the basanite indicates the Li diffusion profile has reached the end of the couple in the 7 min long experiment, attesting to fast diffusion of Li and complicating the “infinite length” assumption of diffusion-couple models. Notably, the $^7\text{Li}/^6\text{Li}$ in mineral grains in the harzburgite vary in a similar manner to that of the glass but lag slightly behind in changing from the $^7\text{Li}/^6\text{Li}$ of starting material to the $^7\text{Li}/^6\text{Li}$ of the glass. Although the measured $^7\text{Li}/^6\text{Li}$ of minerals in the experiment could reflect incorporation of some glass as inclusions, ion intensities during the analysis of the solid were a factor of ~ 3 lower than the nearby glass, consistent with the lower concentration of the minerals relative to the glass based on partitioning (Brenan et al., 1998). The fast approach to isotopic equilibrium indicates that either solid-melt equilibration by diffusion is even more rapid than found experimentally (e.g., for plagioclase; Gilletti and Shanahan, 1998) or that dissolution-precipitation is responsible for equilibration. None of the numerical models shown in Figure 6 provides a particularly good match to the observed $^7\text{Li}/^6\text{Li}$ profile; however, the observed profile is qualitatively consistent with that expected for a noninfinite diffusion couple.

6. DISCUSSION

6.1. The Origin of Large $\delta^7\text{Li}$ Variations in Trinity Peridotite Samples

Our results indicate that Li isotopes can vary significantly over the scale of a single thin section in samples from the Trinity peridotite and, in one case, show extreme variation among single mineral grains. Nevertheless, all three lithologic transects studied produce a systematic pattern in average $\delta^7\text{Li}$ of a thin section as a function of distance from the dunite. The pattern is consistent with the diffusive fractionation of Li isotopes (e.g., Richter et al., 2003) but the extreme diffusive mobility of Li in both high and moderate temperature conditions warrants caution in definitively concluding that magmatic, as opposed to subsolidus, processes created these patterns. The observations are however consistent with creation by isotopic fractionation during magma-based alkali diffusion.

To address the processes affecting the variations in $\delta^7\text{Li}$ at

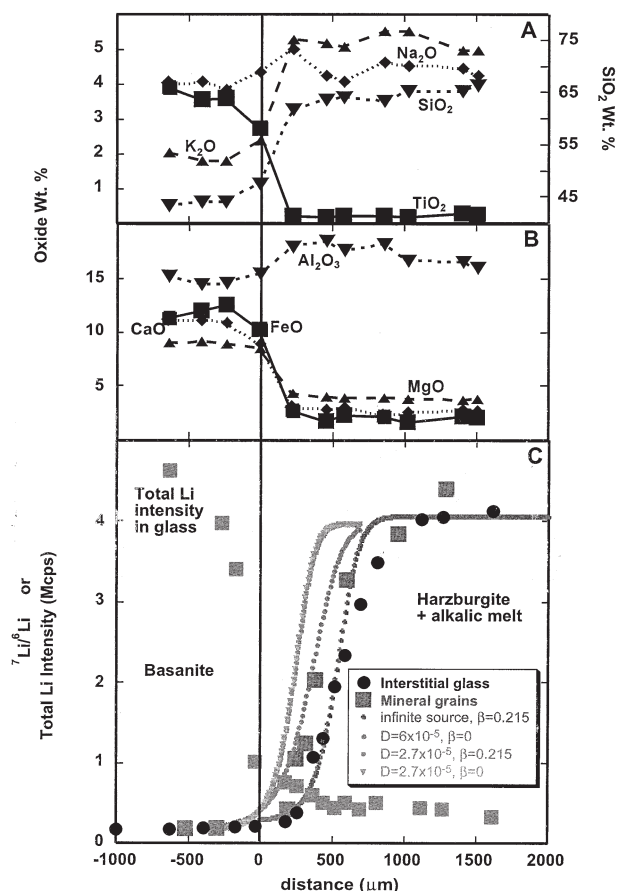


Fig. 6. Elemental variations (A, B) and ${}^7\text{Li}/{}^6\text{Li}$ and Li signal intensity (C) as a function of distance from the initial interface for a 7 min long diffusion-reaction couple in a piston cylinder apparatus. Li analysis data available in GCA AE Table 3; errors are smaller than symbols. The basanite half of the experiment is roughly 80% melt (the rest olivine) while the harzburgite half is $\sim 10\%$ melt. Elemental profiles including that of Li produce binary diffusion profiles crossing the interface at concentration mid points. Note that the absolute intensities of Li in the three analyses of basanite are uncertain because a smaller field aperture was inserted to keep ion intensities low enough to measure using the ion counting system (a correction factor has been applied). ${}^7\text{Li}/{}^6\text{Li}$ smoothly varies across the diffusion couple but the location of this curve is offset from the original interface (shown as line). The distinct offset between the ${}^7\text{Li}/{}^6\text{Li}$ of the initial basanite (0.150 ± 0.001) and that of the basanite spot farthest from the interface (0.177 ± 0.001) indicates that the experiment did not represent an infinite length diffusion couple. The ${}^7\text{Li}/{}^6\text{Li}$ of olivine and orthopyroxenes within the harzburgite only differ slightly from the adjacent melt indicating that solid-melt equilibration is fast. Several models are shown: an infinite reservoir model assuming the source of Li is constant at the interface fails to follow the observed trend. Diffusion couple models using the ${}^7\text{Li}$ diffusion coefficient and β shown also fail to model the data. Constraint on β is not provided by this experiment as illustrated by variation in β producing no discernible difference in model. Models based on a diffusion coefficient dependent on melt SiO_2 content (Richter et al., 2003) also do not reproduce the observed data.

short spatial scales, we begin with discussion of the observations in dunite sample TP90-20-2. The trend of decreasing $\delta^7\text{Li}$ with increasing Li concentration could reflect a surface contaminant in the sample (due to secondary alteration or sample

preparation) that imparts a high $\delta^7\text{Li}$ on minerals with low Li concentration. However, reanalysis of these locations after repolishing and sonication in ultra-pure water continued to produce high $\delta^7\text{Li}$ indicating that this signature was not surface related. Furthermore, analysis of spots on cracks found no systematic difference between crack locations and crack-free locations. Thus, sample contamination does not explain the results.

A nonmagmatic explanation could be that the transect variation pattern reflects an analytical artifact resulting from variation of instrumental mass discrimination with changing clinopyroxene composition across the transect. Such an effect has never been observed during the ion probe analysis of our pyroxene standards having different compositions and mineralogical structure (Beck et al., 2004). In addition, it must be underlined that the observed trough in $\delta^7\text{Li}$ cannot be explained by such an effect because the clinopyroxenes in the dunite and those far from the dunite (in the plagioclase lherzolite; e.g., comparison of VB91-34 and VB91-40) are the most different compositionally, yet have similar isotopic signatures. Indeed, the compositional difference of the two clinopyroxene standards is larger than the difference between clinopyroxenes within the VB91 transect.

Alteration processes must be considered as another possible source for the observed $\delta^7\text{Li}$ variations in TP90-20-2. The trend of higher $\delta^7\text{Li}$ with decreasing Li concentration (Fig. 5) might reflect mixing between the original magmatic $\delta^7\text{Li}$ and seawater ($\delta^7\text{Li} = +32$). However, altered upper oceanic crust shows concomitant increase in Li concentration ($5\text{--}27 \mu\text{g/g Li}$) and $\delta^7\text{Li}$ ($+6\text{--}21$) relative to unaltered MORB (Chan et al., 2002a), unlike the decrease in Li concentration observed in the Trinity samples. The process could also reflect preferential leaching of ${}^6\text{Li}$ from the mineral grains with the high $\delta^7\text{Li}$ -low Li concentration pyroxenes being generally consistent with the inferred effect of serpentinization on Li systematics (Decitre et al., 2002). In fact, this previous ion probe study observed that "relict" minerals generally had lower Li concentrations and higher $\delta^7\text{Li}$ while serpentine and chlorite had higher Li concentrations and lower $\delta^7\text{Li}$. However, the $\delta^7\text{Li}$ vs. Li concentration trends observed in TP90-20-2 show greater change in $\delta^7\text{Li}$ per change in Li concentration compared to the relict-serpentine pairs in Decitre et al. (2002). A strong argument against leaching is that Na_2O contents of Trinity clinopyroxenes are typically 0.2 to 0.4 wt% (Quick, 1981b). If clinopyroxenes were leached of 75% of their original Li as implied by the change in Li content, one might expect similar leaching of Na producing nonstoichiometric pyroxenes; however, this is not observed. Finally, the trends could also reflect mineral interaction with hydrothermal fluids where Li partitioning behavior changes with temperature; however, there is essentially no constraint on this process at present.

The boron isotopic compositions argue against contamination by seawater or seawater derived material. Since the $\delta^{11}\text{B}$ (${}^{11}\text{B}/{}^{10}\text{B}$ relative to a standard) for seawater is $+40$ (Spivack and Edmond, 1987), the $\delta^{11}\text{B}$ of Trinity clinopyroxene having low B concentrations will be extremely sensitive to seawater contamination. Seawater with $72 \mu\text{mol/L B}$ will clearly shift $\delta^{11}\text{B}$ in the clinopyroxenes ($<0.6 \mu\text{g/g B}$) more readily than it shifts $\delta^7\text{Li}$ since seawater has $20 \mu\text{mol/L Li}$ and the CPX have $\mu\text{g/g}$ levels of Li. Within a localized area of TP90-20-2, $\delta^7\text{Li}$ of

clinopyroxene changes from + 5 to + 32 while $\delta^{11}\text{B}$ only ranges from -10 to -15 , or within errors of “mantle” values of Icelandic melts (Gurenko and Chaussidon, 1997) thus arguing against this explanation.

The large fractionations of $^7\text{Li}/^6\text{Li}$ predicted by models suggest that the wide $\delta^7\text{Li}$ variation in TP90-20-2 could reflect an extreme fractionation of Li isotopes during melting. However, consideration of the length scales of subsolidus Li diffusion during the obduction process rules out any magmatic signature being preserved on the scale of a single mineral grain as observed. Indeed, even at 500°C , the diffusive length scales of Li over a million-year obduction process will be ~ 1 cm, greater than the length scale of variation observed. Thus these small-scale variations must reflect a low temperature process occurring after obduction. These observations are consistent with the complexity of Li observed in subaerial weathering processes (Pistiniér and Henderson, 2003).

Regardless of the origin of the $\delta^7\text{Li}$ variation in TP90-20-2, three important points should be emphasized. First, the extreme variability in TP90-20-2 is not observed in any of the other 20 samples we analyzed. Whereas the standard deviation of TP90-20-2 is 10‰, the average standard deviation for all other thin sections is 2.4‰ distinguishing this sample from all others. Second, even if this trend in $\delta^7\text{Li}$ with concentration reflected an alteration process, the original magmatic $\delta^7\text{Li}$ signature should be indicated by the value of $\delta^7\text{Li}$ in the higher Li concentration minerals, which have $\delta^7\text{Li}$ of 0 to + 10. Third, at the larger scale, a systematic relationship between $\delta^7\text{Li}$ and sample position exists for three lithologic transects of different length scale, which is difficult to explain by any alteration process.

Although further work is required to identify the processes affecting Li isotope variability at the micrometer scale in peridotite samples, the observation of a repeated, systematic spatial pattern in $\delta^7\text{Li}$, occurring over decimeter- to meter-length scales, suggests that magmatic diffusion processes are responsible for fractionating Li isotopes. Although the wide variations in $\delta^7\text{Li}$ in sample TP90-20-2 warrant caution in interpretation, the consistent relationship of the spatial pattern with lithologic sequence unambiguously related to magmatic process provides evidence that the thin-section to thin-section variation reflects magmatic processes. As we show below, the observed isotopic signatures are actually quite small compared to what should be expected based on laboratory constrained models of Li isotope fractionation during diffusion.

6.2. Implications of Diffusion-Reaction Experiment

The diffusion-reaction experiment demonstrates that isotopic exchange between the melt and the coexisting mineral phases is nearly instantaneous. Therefore, if diffusion causes fractionations of Li isotopes in a melt, these signatures will be recorded in the coexisting silicate minerals. Thus, for the purposes of our modeling and discussion, we assume that solid-melt equilibrium is instantaneous and that the solid faithfully records changes in the melt composition. Another implication of this experimental result is that Li isotopic exchange between melts and mantle minerals during ascent of magmas will be very rapid and preservation of a $^7\text{Li}/^6\text{Li}$ signature, such as that originally from a slab fluid, is unlikely.

6.3. Models of Alkali Diffusive Fluxing and Advective Extraction of Melt

The creation of the Li isotope profiles by magmatic diffusion processes implies two important points. First, significant fractionations of Li isotopes may occur at mantle temperatures by melt diffusion processes (e.g., Richter et al., 2003); thus variations in $\delta^7\text{Li}$ in basalts do not simply trace source variations introduced by subduction. Second, the isotopic data are qualitatively consistent with alkalis diffusing from melts in dunite conduits to melt in adjacent lherzolite, or from adjacent lherzolite into dunite, implying that the melting process at shallow depths may be affected by diffusion-based melt-rock reactions.

In detail, the observed Li isotope profiles are not consistent with the simple diffusion model given in the introduction (Fig. 1). Such a process should result in decreasing Li concentration away from the dunite whereas Li concentrations either increase or show no trend in composition away from the dunite (Fig. 4). Notably, the distance over which the concentrations of incompatible elements such as the REE increase (e.g., Kelemen et al., 1992) is similar to the distance over which the Li isotope profile occurs (Fig. 2). This observation is inconsistent with a simple diffusion model as the REE will not diffuse as rapidly as Li (Lundstrom, 2003; Richter et al., 2003). To explain both the Li isotope variations and the observed REE concentration patterns requires both a diffusion process and a melt extraction process.

The systematic distribution of Li isotopes and REE concentrations could be explained by a combined process of horizontal alkali diffusion in either direction and extraction of melt from the peridotite back towards the dunite. In one scenario (Fig. 7), alkalis diffuse out of the melt ascending in the conduit to the surrounding peridotite causing the peridotite to melt (Lundstrom, 2000b) and the melt produced is subsequently extracted back to the dunite channel. In this model, diffusion occurs in the direction of the maximum activity gradient, which will be perpendicular to the dunite-harzburgite interface, whereas melt extraction dominantly reflects a vertical buoyancy driving force with a small component of “suction” force pulling melt toward the conduit (Stevenson, 1989; Spiegelman et al., 2001). Although a strong component of horizontal advection would overwhelm any diffusive transport, we assume that the horizontal advection component is small allowing diffusion to control the transport of alkalis away from the dunite melt conduit.

To quantitatively examine this explanation for the observed profiles, we developed a numerical model of combined diffusion and extraction. Our model is a simplification of the inferred process but should capture the essence of the problem, the isotopic fractionation of Li created by diffusion during the continuous extraction of melt. Two assumptions should be pointed out. First, the model only calculates diffusion within a melt and assumes instantaneous equilibrium partitioning with a coexisting solid. Second, the extraction term removes melt and incompatible elements from the system without further interaction with the melt; this term can be viewed as reflecting the net change by vertical advection in the harzburgite and thus accounts for melt advecting from below as well as melt being extracted. We do not attempt to capture the process of near vertical melt ascent and advection back to the melt conduit with a more complex two-dimensional model.

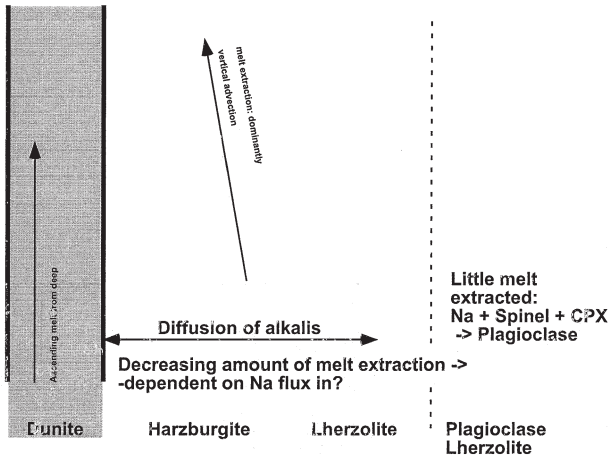


Fig. 7. Schematic diagram showing a hypothesized diffusion-extraction process occurring next to a dunite melt conduit. The plagioclase lherzolite-spinel lherzolite boundary may reflect the location where sodium is still diffusively added but melt is no longer extracted back to the dunite.

To account for melt extraction, a sink term was added to Fick's second law of diffusion (one-dimensional), resulting in the general equation having the following form:

$$\frac{\partial C}{\partial t} = D \frac{\partial^2 C}{\partial x^2} - ACe^{-bx} \quad (1)$$

Here, C is the concentration of a Li isotope (${}^6\text{Li}$ or ${}^7\text{Li}$), which is a function of time and position, D is the diffusion coefficient (particular to a specific isotope), A is the parameterized melt extraction strength and b controls the spatially decaying melt extraction strength. The exponentially decaying extraction strength is chosen here to provide the realism of melts that are closer to the melt conduit being more easily extracted. To analyze the evolution of ${}^6\text{Li}$ and ${}^7\text{Li}$ individually, Eqn. 1 must be applied to the two lithium species separately. Although extraction is applied to the total lithium budget (the sum of the two Li isotopes), the two differential equations remain uncoupled as detailed in the Appendix, where a more detailed formulation and analysis of the governing system is provided. The final nondimensional governing equations are:

$$\frac{\partial C^{Li6}}{\partial t} = \frac{D^{Li6}}{D^{Li7}} \frac{\partial^2 C^{Li6}}{\partial x^2} - \bar{A} \left(C^{Li6} + \frac{C_0^{Li7}}{\Delta C^{Li7}} \right) e^{-bx} \quad (2)$$

$$\frac{\partial C^{Li7}}{\partial t} = \frac{\partial^2 C^{Li7}}{\partial x^2} - \bar{A} \left(C^{Li7} + \frac{C_0^{Li7}}{\Delta C^{Li7}} \right) e^{-bx} \quad (3)$$

with all the variables defined in the Appendix.

We present several permutations of the model to demonstrate the range of parameter variations that could explain the observed data. Important variables and boundary conditions in the model include β , the initial ratio of Li concentrations between the dunite and the rest of the transect, the time over which the process occurs, and the extraction strength (A). We vary the boundary condition of the initial Li concentration ratio, $[\text{Li}]_{\text{dunite}}/[\text{Li}]_{\text{harzburgite}}$ from 1.33 to 0.66 as explained below. It is notable that these small values can create significant Li isotopic variation, and that this ratio

could vary to a greater extent depending on the extent of incremental melting. We also explored a range in β from 0.1 to 0.215 (Richter et al., 2003). The value of b , set to match the observed length scale of the Li and trace element concentration profiles in transect TP90-9, is not varied in our models (all models use $b = 0.2$).

Our assumed range in Li concentration gradient across the dunite-harzburgite boundary reflects two divergent views. On the one hand, we cannot assume the initial concentration gradient was the same as that we have measured in the transects (decreasing incompatible element concentration toward the dunite) because each clinopyroxene only records the last melt in contact with it. Therefore, melts from depth in a polybaric melt column having higher Li contents may have passed through the dunite leading to the assumption in some models that $[\text{Li}]_{\text{dunite}} > [\text{Li}]_{\text{harzburgite}}$. On the other hand, if the concentrations in the dunite clinopyroxenes reflect passage of depleted arc tholeiites through the already transposed oceanic lithosphere (tholeiites that are unrelated to the surrounding lherzolite), the initial concentration gradient could have been $[\text{Li}]_{\text{dunite}} < [\text{Li}]_{\text{harzburgite}}$. Izu arc tholeiites range between 4 and 10 ppm in Li concentrations (Moriguti and Nakamura, 1998) while the average Li clinopyroxene concentration from the two samples farthest from dunite in each of our transects is 3.2 ppm. Assuming equilibrium partitioning between melt and mantle clinopyroxene (Brenan et al., 1998), a melt in the lherzolite would have ~ 11.8 ppm Li, suggesting that $[\text{Li}]_{\text{dunite}} < [\text{Li}]_{\text{harzburgite}}$. Our assumed range of concentration gradients encompasses both of these viable initial situations.

The first models we discuss are for the initial condition $[\text{Li}]_{\text{dunite}}/[\text{Li}]_{\text{harzburgite}} = 1.33$ whereby Li diffuses away from the dunite. Such models allow simultaneous explanation of the trace element concentration profiles and Li isotope profiles and differ from simple diffusion-only models in two important ways: 1) the point of lowest $\delta^7\text{Li}$ (the isotopic trough) does not migrate away from the dunite as rapidly as diffusion-only models; and 2) the magnitude of the trough can increase beyond that determined by β and the original concentration ratio as in the simple diffusion model (Fig. 1). For instance, the trough migrates into the harzburgite at a rate of ~ 2.5 cm/yr in the diffusion only model (Fig. 8) whereas the trough migrates at ~ 0.5 cm/yr using the same diffusion coefficients in the diffusion-extraction model. Depending on the ratio of the extraction term, A , to the Li diffusion coefficient(s), the rate of trough migration in the diffusion-extraction model can go to zero. The slower movement of the trough is explained by the extraction term decreasing the Li concentration in the trough resulting in Li diffusing from the far field lherzolite back toward the trough area. The increase in the magnitude of the $\delta^7\text{Li}$ trough in the diffusion-extraction model relative to the pure diffusion model results from the increase in the concentration gradient from the dunite to the trough. Because Li in the trough is continuously removed, a higher ratio of "diffused-in" Li to original Li can develop. Because Li diffusion occurs in both directions toward the trough, the model predicts a small increase in $\delta^7\text{Li}$ (Fig. 8) beyond the trough in the lherzolite, although this hump may not be resolved in any observational data. Thus, the prediction of the simple diffusion-only model (Fig. 1), that the trough position relative to the dunite is a function of time and that the trough magnitude solely reflects

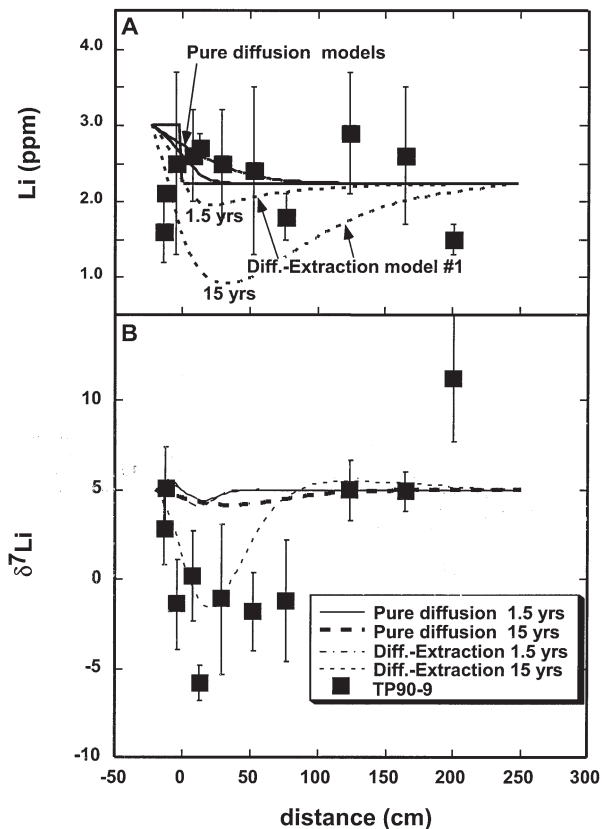


Fig. 8. Comparison of the evolution of Li concentration (A) and $\delta^7\text{Li}$ (B) as a function of distance for a diffusion-only model and a diffusion-extraction model along with data from transect TP90-9. Both models use identical values for the diffusion coefficients of ^7Li and ^6Li and therefore β (which in this model is 0.1). Both models also start with the same concentration ratio ($C_{\text{dunite}}/C_{\text{harzburgite}} = 1.33$) across the dunite-harzburgite interface (at $x = 0$) and the same initial $\delta^7\text{Li}$ of +5 (at all x). Note the difference in the scales of the isotopic shift in the two models: in the model with extraction, a trough of $\delta^7\text{Li} \sim 7\%$ lower than the initial ratio is created after 15 yr while the pure diffusion model only produces a small isotopic shift ($<2\%$). Also note that the diffusion-extraction model produces a more narrow trough which moves away from the dunite-harzburgite interface at a slower rate than the diffusion-only model (whose migration with time is best illustrated in Fig. 1). Although the diffusion-extraction model here uses conservative values for β and $C_{\text{dunite}}/C_{\text{harzburgite}}$ both of which minimize any isotopic fractionation, the model shown for 15 yr can reproduce the values of $\delta^7\text{Li}$ observed in transect TP90-9.

the initial Li concentration ratio and β , is opposite to the prediction of the diffusion-extraction model, where the trough position is relatively stationary but the magnitude of the trough increases with time.

Observations from the lithologic transects in the Trinity peridotite are consistent with the diffusion-extraction model but inconsistent with a diffusion-only model. For example, the relative positions of the $\delta^7\text{Li}$ trough for each transect do not vary appreciably despite the lengths of the three transects varying by two orders of magnitude. The position of the lowest $\delta^7\text{Li}$ in each transect remains close to the boundary between harzburgite and dunite (5, 13 and 100 cm from the boundary) in the 20, 200 and 2000 cm transects, respectively. The distinction in $\delta^7\text{Li}$ behavior between these models cannot be

overstated; whereas the $\delta^7\text{Li}$ of a diffusion only model is essentially fixed by β and the initial concentration ratio, the diffusion-extraction model allows a greater range in $\delta^7\text{Li}$ by creating greater concentration gradients and reducing the dilution effect of the original Li in the harzburgite reservoir.

This first iteration of our diffusion-extraction model (Model 1) shown in Figure 8 could be considered a conservative case as it uses β of 0.1, a low concentration ratio (1.33), and low diffusion coefficients. In contrast, using the recent experimentally determined values of β and D_{Li} (Richter et al., 2003), large shifts in Li isotope composition are readily produced by our diffusion-extraction model. In this model iteration (Richter Model shown in Fig. 9), the observed magnitude of the TP90-9 trough can be matched in just 1.5 yr with a 30‰ fractionation predicted after 15 yr. In detail, the marked increase in fractionation in this model relative to the first diffusion-extraction model (model #1) reflects the ratio of the diffusive flux into the trough area over the extraction flux (Fig. 10) with the model using the Richter diffusion coefficients having a higher ratio for a given model time. Note that the profile of the 15 yr model reaches the limit of the boundary condition and is probably a minimum estimate of the isotopic fractionation. As explained below, diffusive relaxation during the ophiolite obduction process will also be significant and this effect could lessen the observed concentration and $\delta^7\text{Li}$ gradients relative to that produced originally by the melting process.

The extraction rates used in the Li models should be consistent with the observed profiles of other nondiffusively affected elements. Although model #1 can reproduce the Nd profile of transect TP90-9 using the same value of A for Li and Nd, the Richter diffusion-extraction model requires that A for Nd is $10\times$ less than that of Li ($A = 5 \times 10^{-9}$, Fig. 9) to match both profiles. This difference between Nd and Li extraction rate may not be realistic given the partitioning behavior of each element. Li has similar mineral/melt partition coefficients for olivine, orthopyroxene and clinopyroxene (Brenan et al., 1998) such that its bulk partitioning is relatively insensitive to lithology or mode. In contrast, the bulk partition coefficient for Nd will strongly depend on the clinopyroxene mode so that the bulk D for Nd should be less than that of Li. Thus, whereas a higher extraction rate for Nd should be expected, the Richter model suggests the opposite.

The alternative initial condition is that $[\text{Li}]_{\text{dunite}}/[\text{Li}]_{\text{harzburgite}} < 1$, consistent with the observed Li concentration profile in the transect TP90-20. The development of this model with time can be seen in comparing the 1.5 and 15 yr models (Fig. 11). After 1.5 yr, Li has diffused from the harzburgite to the dunite producing a high in $\delta^7\text{Li}$ in the harzburgite and a small trough near the dunite. However, as extraction proceeds to create a low in Li concentration in the trough, $\delta^7\text{Li}$ evolves in 15 yr to a trough similar to previous models which had $[\text{Li}]_{\text{dunite}}/[\text{Li}]_{\text{harzburgite}} > 1$. This behavior emphasizes that the important aspect of this model is the extraction term, which will magnify diffusive isotopic fractionation, and not the direction that Li diffuses. Given the same concentration gradients, a diffusion-only model in the direction harzburgite-dunite will produce $\delta^7\text{Li}$ variations similar to that seen in the pure diffusion model in Figure 8, $\sim 2\%$.

The assumption of using $[\text{Li}]_{\text{dunite}}/[\text{Li}]_{\text{harzburgite}} > 1$ is that early formed “deep” melts ascend in the dunite conduit and

thus should have higher Li contents than the melt in the shallow depleted peridotite. However, dunites generally are observed to have lower incompatible element concentrations; this can be explained by dunites experiencing the greatest melt flux and

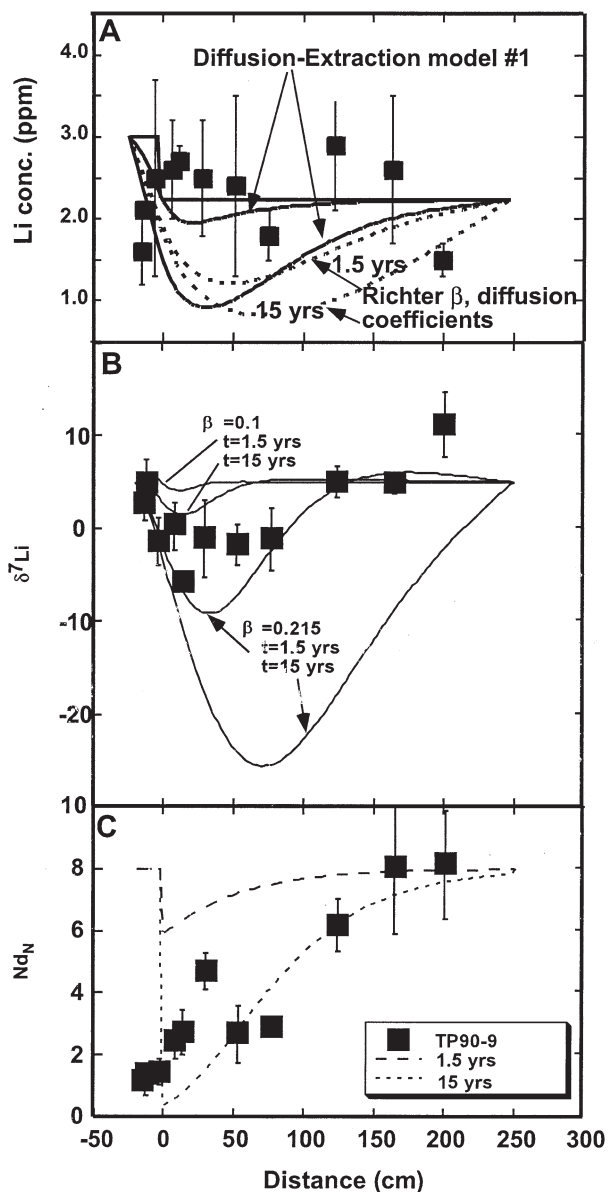


Fig. 9. Evolution of Li concentration (A), $\delta^7\text{Li}$ (B), and Nd concentration (C) in a diffusion-extraction model using the Li diffusion coefficients of Richter et al. (2003), where $\beta = 0.215$. For comparison, the diffusion-extraction model using $\beta = 0.1$ given in Figure 8 is also shown. Very large changes in $\delta^7\text{Li}$ are predicted using the higher value of β with $>30\%$ found in the 15 yr model. Note that because the isotopic profile has approached the outer boundary condition at 250 cm, this model may underestimate the fractionation. This model uses the same initial concentration ratio between the dunite and harzburgite (see text). This model indicates that variations in $\delta^7\text{Li}$ much larger than those observed in the Trinity transects can be produced in models using realistic parameters. In order for the Richter model to explain both the Li and Nd behavior, A for Nd must be $10\times$ less than that of Li ($A = 5 \times 10^{-9}$); in model #1 (not shown), the same value of A for Li and Nd allow matching of both profiles.

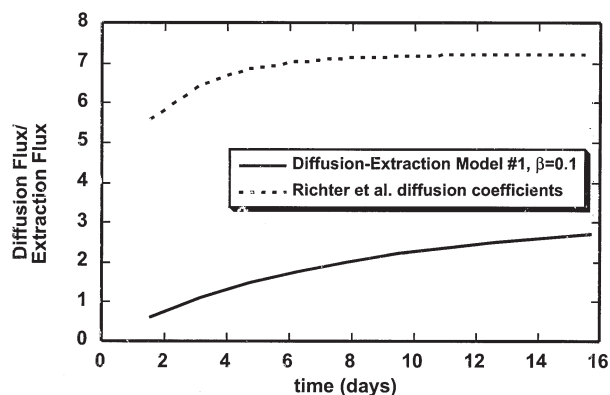


Fig. 10. Ratio of diffusive flux to extraction flux as a function of model calculation time. Two models are shown, diffusion-extraction model #1 and the Richter diffusion-extraction model. The increase in the size of the $\delta^7\text{Li}$ trough observed in the Richter diffusion-extraction model is explained by the larger diffusive flux to extraction flux ratio of this model. The diffusive flux reflects the amount of Li diffused across the two boundary conditions (at far left and far right); all diffusion between these is treated as only a rearrangement of Li and is not included in diffusive flux. Extraction flux reflects the integration of all Li extracted between the dunite-harzburgite boundary and the far-field horizontal boundary in the harzburgite.

amount of element extraction and therefore evolving to the lowest Li concentrations with time, particularly as the conduit system shuts down. With this in mind, we tested one final model (Fig. 11) where the dunite boundary condition evolves through time starting with $[\text{Li}]_{\text{dunite}}/[\text{Li}]_{\text{harzburgite}}$ of 1.33 and changing to 0.66 over the 15 yr interval. Although this model introduces one more free parameter, it is consistent with both the observed patterns in $\delta^7\text{Li}$ and Li concentration throughout the transect. Note that both of these models use the Richter values for D and β , yet have $\delta^7\text{Li}$ troughs significantly smaller than the diffusion-extraction model in Figure 9.

One goal of our modeling is to constrain the timescale over which melt may have fluxed through a dunite conduit. Our model has explored a range of time from 1.5 to 15 yr, although there is little outside constraint on how long the melt transport process in a melt conduit might last. Comparisons of permutations of the model (not shown) indicate that one can simply balance off changes in the diffusion and extraction parameters with the time of the process. For instance, two model variations using different parameters, one with $D_{\text{Li}} = 2 \times 10^{-6} \text{ cm}^2/\text{s}$, $A = 2 \times 10^{-9}$, and $t = 15.7 \text{ yr}$, the other with $D_{\text{Li}} = 2 \times 10^{-7} \text{ cm}^2/\text{s}$, $A = 2 \times 10^{-10}$, $t = 157 \text{ yr}$ produce identical $\delta^7\text{Li}$ profiles with distance. Given our experimental result showing fast equilibration between melt and coexisting minerals, an effective diffusion coefficient for Li (combining both melt diffusion and mineral uptake) of $10^{-6} \text{ cm}^2/\text{s}$ or less is probably appropriate indicating year to decade timescales of conduit life.

One final observation providing evidence for a diffusion-based melt-peridotite interaction process is the behavior of Sr within transect TP90-9. Although concentrations of REE decrease approaching the dunite as expected for increasing amounts of melt extraction, concentrations of Sr actually increase approaching the dunite despite the fact that the bulk distribution coefficient for Sr should be similar to that of Nd (Fig. 2c). This feature could be explained by the development

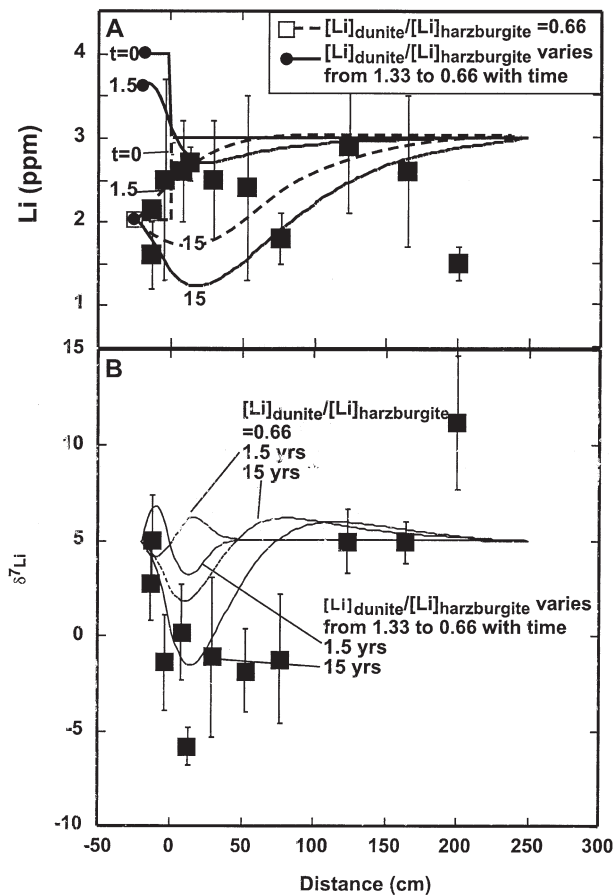


Fig. 11. Li concentration (A) and $\delta^7\text{Li}$ profiles (B) in diffusion-extraction models using different $[\text{Li}]_{\text{dunite}}/[\text{Li}]_{\text{harzburgite}}$. In the first model, a constant $[\text{Li}]_{\text{dunite}}/[\text{Li}]_{\text{harzburgite}}$ of 0.66 is used; in the first 1.5 yr, Li diffuses from the harzburgite to the dunite resulting in a small high in $\delta^7\text{Li}$ in the harzburgite. However, as extraction proceeds, it creates a low in Li concentration adjacent to the dunite and $\delta^7\text{Li}$ evolves in 15 yr to a trough similar to other models in which $[\text{Li}]_{\text{dunite}}/[\text{Li}]_{\text{harzburgite}} > 1$. A second model examines the scenario where ascending melts in the conduit have high Li concentrations early in the conduit life but evolve to lower concentrations near the end of the conduit's life; here, $[\text{Li}]_{\text{dunite}}/[\text{Li}]_{\text{harzburgite}}$ changes from 1.33 to 0.66 over the 15 yr interval.

of a boundary layer at the interface between the melt conduit and the surrounding peridotite. In laboratory diffusion-reaction experiments, Ca from the peridotite diffuses toward the interface between the basalt and the partially molten peridotite, resulting in a melt with high CaO concentrations building up in a boundary layer within the interface region (Lundstrom, 2003). Given the similar chemical behaviors of Sr and Ca, it is possible that Sr may also become enriched in this region, thus producing the observed Sr profile.

The Li isotopic profiles indicate alkali diffusion may influence melting of peridotite around a dunite melt conduit. Diffusion of Na into the surrounding peridotite at shallow depths will dramatically increase melt production of the peridotite (e.g., Hirschmann, 2000) while the loss of Na from the melt in the dunite conduit will decrease melt mass proportionately less (through crystallization in the conduit). Indeed, Gruau et al. (1995) has pointed out that the major lithologic variations in the

Trinity peridotite reflect melt-rock interaction, not decompression melting. If the melt rock reaction zones reflect alkali diffusion at shallow depths, this process could be important to shaping the composition of both erupted magmas and residual peridotites.

The diffusion-extraction model illustrates how sensitive Li isotope variations can be to diffusive processes. However, any $\delta^7\text{Li}$ profile developed during magmatic processes may also be affected by postmagmatic processes such as obduction. The ophiolite obduction process probably involves a slow cooling process such that the magmatic $\delta^7\text{Li}$ and Li concentration profile could be affected by diffusional homogenization during obduction. Li diffusion rates in clinopyroxene and olivine are not presently known which limits the ability to assess this robustly. However, Li diffusion in plagioclase is exceedingly fast with a D of $\sim 10^{-13}$ m^2/s at 873 K (Gilletti and Shanahan, 1997). If obduction took 1 million years, the length scale of diffusional homogenization using this D would be ~ 1.7 m, erasing the lithologic variations in $\delta^7\text{Li}$ observed here. However, diffusion of Li in olivine or clinopyroxene is probably much slower than in plagioclase. In plagioclase, Li is much smaller than the major cations Na and Ca determining the site size, resulting in its high diffusivity. In contrast, the ionic radius of Li is very similar to that of Mg, the major cation occupying its host site in clinopyroxene or olivine. Because size misfit affects the elastic strain of a cation (diffusion model of Van Orman et al., 2001), D_{Li} in these minerals should be several orders of magnitude less than 10^{-13} m^2/s . If it is four orders of magnitude lower, the length scale of homogenization would be only 1.7 cm, which would not erase the observed profiles. Another aspect to consider is the concentration gradients that drive Li diffusion during this process. Because there is not a large or even clear Li concentration gradient (e.g., transects TP90-9 and VB-91) toward or away from the dunite, predicting the extent of low temperature diffusive relaxation is difficult. Clearly, constraint on Li diffusion through these minerals is needed for better assessment of this effect.

6.4. Implications for Li Isotope Geochemistry and Li Geochemical Cycles

The observation of 10‰ variations in $\delta^7\text{Li}$ within mantle peridotites is problematic in two somewhat contradictory ways. On the one hand, the observed variation in $\delta^7\text{Li}$ is large relative to the range observed in mantle basalts. On the other hand, laboratory experiments and models examining Li diffusion and diffusive fractionation imply that variations in $\delta^7\text{Li}$ much larger than those observed might be expected.

The range in average $\delta^7\text{Li}$ in mantle-derived magmas is surprisingly narrow. For instance, $\delta^7\text{Li}$ in unaltered MORB varies only slightly, between +3.4 and +4.7‰ (Chan et al., 1992) and ranges by $\sim \pm 1.5$ ‰ for East Pacific Rise MORB (Elliott et al., 2002). In subduction zone magmas, possibly more relevant to the Trinity ophiolite if it formed in a back arc setting, the range in $\delta^7\text{Li}$ can be slightly higher, from +1.1 to +7.6‰ as in the Izu arc (Moriguti and Nakamura, 1998), from +1.4 to +11.2‰ as in Panama (Tomascak et al., 2000), from +0.7 to +7.6‰ as in the Marianas (Benton and Tera, 2000) or can be near constant as in Central America (Chan et al., 2002b).

In contrast, melt inclusions, which sample magmas on a spatial scale similar to that of this study, show much greater variability in $\delta^7\text{Li}$ (Sobolev et al., 2002). Few published analyses of Li isotopes in mantle peridotite exist for comparison. One Zabargad Island peridotite has MORB-like $\delta^7\text{Li}$ (Chan et al., 2002a) while more recent work found mantle samples in Zabargad ranging between -4.2‰ and $+11.8\text{‰}$ (Brooker et al., 2004). Peridotite xenoliths from Japan and Australia show wide variations ranging from $\delta^7\text{Li}$ as low as -17‰ in Japan vs. $+5\text{‰}$ in Australia (Nishio et al., 2004). Thus, the relative variability in peridotites and melt inclusions is consistently greater than that in volcanic rocks. This difference probably results from two contributing factors. First, the extreme rate of Li diffusion in melts results in fast homogenization during the ubiquitous magma mixing process. Second, the diffusion processes occurring adjacent to a melt conduit would be important for affecting the $\delta^7\text{Li}$ of the solid peridotite but may not greatly affect the $\delta^7\text{Li}$ of the ascending melts due to the high melt/rock ratios through the conduit and the incompatibility of Li in the solid relative to the melt.

If the diffusive flux of Li into the mantle and even the crust surrounding a conduit for melt ascent is volumetrically significant, this process could represent an important control on the mass balance of Li isotopes for the planet. If so, the transfer of Li from the mantle to the crust could create a significant Li isotopic fractionation. During the alkali diffusion process described here, every magma ascending through a conduit system will lose a slight amount of ^6Li relative to ^7Li because the ^6Li will diffuse farther from the zone of melt extraction. Over the time of one eruption, this loss may not be significant. However, extrapolating such a process over the timescales of earth differentiation, such a process could produce a greater “effective partition coefficient” for ^6Li than ^7Li resulting in the seawater/crust reservoir having on average a higher $\delta^7\text{Li}$ than that of the mantle or of chondrites ($0 \pm 4\text{‰}$, James and Palmer, 2000; McDonough et al., 2003). Such a planetary scale isotope fractionation between the crust and mantle would not imply a significant secular change in the evolution of the $\delta^7\text{Li}$ of the mantle because the amount of Li transferred from the mantle to the crust represents only a few percent of the total initial mantle Li.

7. CONCLUSIONS

Large variations in $^7\text{Li}/^6\text{Li}$ occur across three different dunite to plagioclase lherzolite transects within the Trinity peridotite in northern California. Average values for $\delta^7\text{Li}$ for single thin sections along the traverse produce a $\sim 10\text{‰}$ decrease in $\delta^7\text{Li}$ in the harzburgite adjacent to the dunite returning to higher values farther from the dunite. This pattern is consistent with a process whereby Li isotopes are fractionated during Li diffusion, either from a melt within a dunite out to the surrounding peridotite or from a melt in the peridotite back into the dunite conduit. The pattern occurs over a length scale similar to the decrease in REE concentration from these same samples (Kelemen et al., 1992). A combined process of diffusion of Li and extraction of melt back into the conduit can reproduce the observed isotopic patterns with Li diffusing in either direction. Models using experimentally constrained values for the relative diffusion rates of ^6Li and ^7Li show that fractionations of more than 30‰

are readily created by passage of melt over year to decade timescales.

Acknowledgments—We thank Tim Elliott, Paul Tomascak and Frank Richter for thoughtful reviews, and A. Brandon for careful editing. CCL thanks Jinju Lee and Judy Baker for technical assistance with the UIUC SIMS and Fang Huang for help with modal analyses. UIUC SIMS analyses were carried out in the Center for Microanalysis of Materials, University of Illinois, which is partially supported by the U.S. Department of Energy under grant DEFG02-91-ER45439. This work was supported by NSF OCE0096533.

Associate editor: A. Brandon

REFERENCES

- Aharonov E., Spiegelman M., and Kelemen P. (1997) Three-dimensional flow and reaction in porous media: Implications for the Earth's mantle and sedimentary basins. *J. Geophys. Res.* **102**, 14821–14833.
- Asimow P. D. (1999) A model that reconciles major- and trace-element data from abyssal peridotites. *Earth Planet. Sci. Lett.* **169**, 303–319.
- Beck P., Barrat J. A., Chaussidon M., Gillet P., and Bohn M. (2004) Li isotopic variations in single pyroxenes from the NWA 480 shergottite: A record of degassing of Martian magmas? *Geochim. Cosmochim. Acta, Geochim. Cosmochim. Acta* **68**, 2925–2933.
- Benton L. and Tera F. (2000) Lithium isotope systematics of the Marianas revisited abstract 10th V.M. Goldschmidt Conference (Cambridge Publications). *J. Conf. Abstr.* **5**, 210.
- Brenan J. M., Neroda E., Lundstrom C. C., Shaw H. F., Ryerson F. J., and Phinney D. L. (1998) Behavior of boron, beryllium and lithium during melting and crystallization: Constraints from mineral-melt partitioning experiments. *Geochim. Cosmochim. Acta* **62**, 2129–2141.
- Brooker R., Blundy J., and James R. (2004) Trace elements and Li isotope systematics in Zabargad peridotites: evidence of ancient subduction processes in the Red Sea Mantle. *Chem Geol.* **212**, 179–204.
- Chan L. H. and Edmond J. M. (1988) Variation of lithium isotope composition in the marine environment: A preliminary report. *Geochim. Cosmochim. Acta* **52**, 1711–1717.
- Chan L. H., Edmond J. M., Thompson G., and Gillis K. (1992) Lithium isotopic composition of submarine basalts—Implications for the lithium cycle in the oceans. *Earth Planet. Sci. Lett.* **108**, 151–160.
- Chan L. H., Alt J. C., and Teagle D. A. H. (2002a) Lithium and lithium isotope profiles through the upper oceanic crust; a study of seawater-basalt exchange at ODP Sites 504B and 896A. *Earth Planet. Sci. Lett.* **201**, 187–201.
- Chan L. H., Leeman W. P., and You C. F. (2002b) Lithium isotopic composition of Central American volcanic arc lavas: Implications for modification of subarc mantle by slab-derived fluids; correction. *Chem. Geol.* **182**, 293–300.
- Chaussidon M. and Marty B. (1995) Primitive boron isotope composition of the mantle. *Science* **269**, 383–386.
- Chaussidon M. and Robert F. (1998) $^7\text{Li}/^6\text{Li}$ and $^{11}\text{B}/^{10}\text{B}$ variations in chondrules from the Semarkona unequilibrated chondrite. *Earth Planet. Sci. Lett.* **164**, 577–589.
- Chaussidon M. and Robert F. (1999) Lithium nucleosynthesis in the Sun inferred from the Solar wind $^7\text{Li}/^6\text{Li}$ ratio. *Nature* **402**, 270–274.
- DeCitre S. E., Deloue L., Reisberg R., James R., Agrinier P., and Mevel C. (2002) Behavior of Li and its isotopes during serpentinization of oceanic peridotites. *Geochem. Geophys. Geosyst.* **10.1029/2001GC000178**.
- Dick H. J. B. and Natland J. H. (1996) Late-stage melt evolution and transport in the shallow mantle beneath the East Pacific Rise. Proceedings of the Ocean Drilling Program, Scientific Results, volume 147 (eds. C. Mevel, K. M. Gillis, J. F. Allan, and P. S. Meyer), 103–134.
- Elliott T., Thomas A. L., Jeffcoate A. B., and Niu Y. (2002) Li isotope variations in the upper mantle. abstract A214 In *Twelfth Annual V. M. Goldschmidt Conference*. Cambridge University Press.

- Gilletti B. J. and Shanahan T. M. (1997) Alkali diffusion in plagioclase feldspar. *Chem. Geol.* **139**, 3–20.
- Gruau G., Lecuyer C., Bernard-Griffiths J. and Morin N. (1991) Origin and petrogenesis of the Trinity Ophiolite Complex (California): New constraints from REE and Nd isotope data. In *Orogenic Lherzolites and Mantle Processes* (eds. M. A. Menzies, C. Dupuy and A. Nicolas), pp. 229–242. J. Petrology Spec. Vol. Oxford University Press, USA.
- Gruau G., Bernard-Griffiths J., Lecuyer C., Henin O., Mace J., and Cannat M. (1995) Extreme Nd isotopic variation in the Trinity ophiolite complex and the role of melt/rock reactions in the oceanic lithosphere. *Contrib. Mineral. Petrol.* **121**, 337–350.
- Gurenko A. A. and Chaussidon M. (1997) Boron concentrations and isotopic composition of the Icelandic mantle; evidence from glass inclusions in olivine. *Chem. Geol.* **135**, 21–34.
- Hirschmann M. M., Baker M. B., and Stolper E. M. (1998) The effect of alkalis on the silica content of mantle-derived melts. *Geochim. Cosmochim. Acta* **62**, 883–902.
- Hirschmann M. M. (2000) Mantle solidus: Experimental constraints and the effect of peridotite compositions. *Geochem. Geophys. Geosyst.*, 2000GC000070.
- Holtzman B. K., Kohlstedt D. L., Zimmerman M. E., Heidelbach F., Hiraga T., and Hustedt J. (2003) Melt segregation and strain partitioning: Implications for seismic anisotropy and mantle flow. *Science* **301**, 1227–1230.
- Jacobsen S. B., Quick J. E., and Wasserburg G. J. (1984) A Nd and Sr isotopic study of the Trinity Peridotite; implications for mantle evolution. *Earth Planet. Sci. Lett.* **68**, 361–378.
- James R. H. and Palmer M. R. (2000) The lithium isotope composition of international rock standards. *Chem. Geol.* **166**, 319–326.
- Johnson K. T. M., Dick H. J. B., and Shimizu N. (1990) Melting in the oceanic upper mantle: An ion microprobe study of diopsides in abyssal peridotites. *J. Geophys. Res.* **95**, 2661–2678.
- Jull M., Kelemen P. B., and Sims K. (2002) Consequences of diffuse and channelled porous melt migration on uranium series disequilibria. *Geochim. Cosmochim. Acta* **66**, 4133–4148.
- Kelemen P. B., Dick H. J. B., and Quick J. E. (1992) Formation of harzburgite by pervasive melt rock reaction in the upper mantle. *Nature* **358**, 635–641.
- Kelemen P. B., Shimizu N., and Salters V. J. M. (1995) Extraction of mid-ocean-ridge basalt from the upwelling mantle by focused flow of melt in dunite channels. *Nature* **375**, 747–753.
- Kelemen P. B., Hirth G., Shimizu N., Spiegelman M., and Dick H. J. B. (1997) Review of melt migration processes in the adiabatically upwelling mantle beneath oceanic spreading ridges. *Phil. Trans. R. Soc. Lond. Ser. A* **355**, 283–318.
- Kelemen P. B., Braun M., and Hirth G. (2000) Spatial distributions of melt conduits in the mantle beneath oceanic spreading ridges: Observations from the Ingalls and Oman ophiolites. *Geochem. Geophys. Geosyst.* **1**, 1999GC000012.
- Kushiro I. (1975) On the nature of silicate melt and its significance in magma genesis: Regularities in the shift of the liquidus boundaries involving olivine, pyroxene and silica minerals. *Am. J. Sci.* **275**, 411–431.
- Lanphere M. A., Irwin W. P., and Hotz P. E. (1968) Isotopic age of the Nevadan orogeny and older plutonic and metamorphic events in the Klamath Mountains, California. *Geol. Soc. Am. Bull.* **79**, 1027–1052.
- Lundstrom C. C. (2000a) Models of U-series disequilibria generation in MORB: The effect of two scales of melt porosity. *Phys. Earth Planet. Int.* **121**, 189–204.
- Lundstrom C. C. (2000b) Rapid diffusive infiltration of sodium into partially molten peridotite. *Nature* **403**, 527–530.
- Lundstrom C. C. (2003) An experimental investigation of the diffusive infiltration of alkalis into partially molten peridotite: Implications for mantle melting process. *Geochem. Geophys. Geosyst.* DOI10.1029/2001GC000224.
- McDonough W. F., Teng F. Z., Tomascak P. B., Ash R. D., Grossman J. N., and Rudnick R. L. (2003) Lithium isotopic composition of chondritic meteorites. *LPSC* **34**.
- Moriguti T. and Nakamura E. (1998) Across-arc variation of Li isotopes in lavas and implications for crust/mantle recycling at subduction zones. *Earth Planet. Sci. Lett.* **163**, 167–174.
- Mungall J. E. (2002) Empirical models relating viscosity and tracer diffusion in magmatic silicate melts. *Geochim. Cosmochim. Acta* **66**, 125–143.
- Navon O. and Stolper E. (1987) Geochemical consequences of melt percolation: The upper mantle as a chromatographic column. *J. Geol.* **95**, 285–307.
- Nishio Y., Nakai S., Yamamoto J., Sumino H., Matsumoto T., Prikhodko V. S., and Arai S. (2004) Lithium isotopic systematics of the mantle-derived ultramafic xenoliths: Implications for EM1 origin. *Earth Planet. Sci. Lett.* **217**, 245–261.
- O'Hara M. J. (1968) The bearing of phase equilibria studies in synthetic and natural systems on the origin and evolution of basic and ultrabasic rocks. *Earth Science Rev.* **4**, 69–133.
- Pistiner J. S. and Henderson G. M. (2003) Lithium-isotope fractionation during continental weathering processes. *Earth Planet. Sci. Lett.* **214**, 327–339.
- Quick J. E. (1981a) The origin and significance of large, tabular dunite bodies in the Trinity Peridotite, northern California. *Contrib. Mineral. Petrol.* **78**, 413–422.
- Quick J. (1981b) Petrology and petrogenesis of the Trinity Peridotite, an upper mantle diapir in the eastern Klamath mountains, Northern California. *J. Geophys. Res.* **86**, 11837–11863.
- Richter F. M., Liang Y., and Davis A. M. (1999) Isotope fractionation by diffusion in molten oxides. *Geochim. Cosmochim. Acta* **63** (18), 2853–2861.
- Richter F. M., Davis A. M., DePaolo D. J., and Watson E. B. (2003) Isotope fractionation by chemical diffusion between molten basalt and rhyolite. *Geochim. Cosmochim. Acta* **67**, 3905–3923.
- Ryan J. G. and Langmuir C. H. (1987) The systematics of lithium abundances in young volcanic rocks. *Geochim. Cosmochim. Acta* **51**, 1727–1741.
- Smith G. D. (1978) *Numerical Solution of Partial Differential Equations: Finite Different Methods*. 2nd ed Oxford University Press.
- Sobolev A. V., Hofmann A., Shimizu N., Chaussidon M., Metrich N., Nikogosian I. K., and Anderson A. T. (2002) Primary melts reveal small scale heterogeneity in convection mantle. Abstract A72S In *Twelfth Annual V. M. Goldschmidt Conference*. Cambridge University Press.
- Spiegelman M., Kelemen P. B., and Aharonov E. (2001) Causes and consequences of flow organization during melt transport; the reaction infiltration instability in compactible media. *J. Geophys. Res.* **106**, 2061–2077.
- Spivack A. J. and Edmond J. (1987) Boron isotope exchange between seawater and the oceanic crust. *Geochim. Cosmochim. Acta* **51**, 1033–1043.
- Stevenson D. J. (1989) Spontaneous small-scale melt segregation in partial melts undergoing deformation. *Geophys. Res. Lett.* **16**, 1067–1070.
- Stolper E. M. (1980) A phase diagram for mid-ocean ridge basalts: Preliminary results and implications for petrogenesis. *Contrib. Mineral. Petrol.* **74**, 13–27.
- Sun S. and McDonough W. F. (1989) Chemical and isotopic systematics of ocean basalts: Implications for mantle composition and processes. In *Magmatism in the Ocean Basins* (eds. A. D. and Saunders M. J. Norry), pp. 313–345. Blackwell Scientific.
- Teng F. Z., McDonough W. F., Rudnick R. L., Dalpe C., Tomascak P. B., Gao S., and Chappell B. W. (2004) Lithium isotopic composition and concentration of the upper continental crust. *Geochim. Cosmochim. Acta*, **68**, 4167–4178.
- Tomascak P. B. (2004) Developments in the understanding and application of lithium isotopes in the Earth and planetary sciences. In *Geochemistry of Non-Traditional Isotope Systems* (eds. C. Johnson, B. Beard and F. Albarede). MSA Reviews in Mineralogy and Geochemistry 55. Mineralogical Society of America, Washington, D.C. pp. 153–195.
- Tomascak P. B., Tera F., Helz R. T., and Walker R. J. (1999) The absence of lithium isotope fractionation during basalt differentiation; new measurements by multicollector sector ICP-MS. *Geochim. Cosmochim. Acta* **63**, 907–910.
- Tomascak P. B., Ryan J. G., and Defant M. J. (2000) Lithium isotope evidence for light element decoupling in the Panama subarc mantle. *Geology* **28**, 507–510.

Van Orman J. A., Grove T. L., and Shimizu N. (2001) Rare earth element diffusion in diopside; influence of temperature, pressure, and ionic radius and an elastic model for diffusion in silicates. *Contrib. Mineral. Petrol.* **141**, 687–703.

SUPPLEMENTARY DATA

Supplementary data associated with this article can be found, in the online version, at doi:10.1016/j.gca.2004.08.004.

APPENDIX

Mathematical Formulation of the Diffusion of Lithium Isotopes with Extraction

In this analysis, we assume that melt extraction takes on an exponential form with distance to reflect the fact that the extraction strength decays as a function of the distance from the dunite. Also, extraction is also a function of the local lithium concentration such that no extraction will take place in the absence of any lithium. Consequently, extraction takes on the following form.

$$AC^{Li}e^{-bx} \quad (A1)$$

Here, A is the amplitude of the extraction, and b is the decaying constant. Both A and b are treated as parameters to be determined by the observed data. CLi is the local lithium concentration, which is the sum of the ⁶Li and ⁷Li concentrations. Thus,

$$C^{Li} = C^{Li6} + C^{Li7} \quad (A2)$$

where C^{Li6} and C^{Li7} are the concentrations for ⁶Li and ⁷Li, respectively. It follows that the governing equations for diffusion and extraction of ⁶Li and ⁷Li are given below. Because advective melt extraction applies to the total local lithium concentration, the amount of lithium to be extracted is $A(C^{Li6} + C^{Li7})e^{-bx}$. Availability of each individual species to be extracted is determined by the local concentration ratio. Consequently, the amount of an individual species to be extracted at any x becomes $A(C^{Li6} + C^{Li7})e^{-bx} \times [C^{Li6}/(C^{Li6} + C^{Li7})] = AC^{Li6}e^{-bx}$, where y can either be 6 or 7 depending on which species is being considered.

$$\frac{\partial C^{Li6}}{\partial t} = D^{Li6} \frac{\partial^2 C^{Li6}}{\partial x^2} - AC^{Li6}e^{-bx} \quad (A3)$$

$$\frac{\partial C^{Li7}}{\partial t} = D^{Li7} \frac{\partial^2 C^{Li7}}{\partial x^2} - AC^{Li7}e^{-bx} \quad (A4)$$

Here, D^{Li6} and D^{Li7} are the diffusion coefficients for ⁶Li and ⁷Li, respectively. Eqns. A3 and A4 represent two uncoupled governing equations for the diffusion and extraction of C^{Li6} and C^{Li7} . Next, let us factor out C^{Li6} and C^{Li7} , respectively, from Eqns. A3 and A4. The

governing equations become the following. We also note that under normal conditions, $C^{Li7}/C^{Li6} \cong 12.1163$.

Following a standard procedure to seek numerical solutions for the governing Eqns. A3 and A4, these equations are nondimensionalized by introducing the following nondimensional variables.

$$C' = \frac{C - C_0^{Li7}}{\Delta C^{Li7}}; \quad x' = \frac{x}{L}; \quad t' = t \frac{D^{Li7}}{L^2} \quad (A5)$$

Here, C_0^{Li7} is the constant reference ⁷Li concentration in the dunite; ΔC^{Li7} is the concentration difference of ⁷Li between the dunite and the far field harzburgite units; and L is the half width of the dunite unit. After substituting the nondimensional variables into the governing equations together with some algebraic manipulations, the following nondimensional governing equations are obtained. In this set of nondimensional governing equations, the primes have been dropped for simplicity.

$$\frac{\partial C^{Li6}}{\partial t} = \frac{D^{Li6}}{D^{Li7}} \frac{\partial^2 C^{Li6}}{\partial x^2} - \bar{A} \left(C^{Li6} + \frac{C_0^{Li7}}{\Delta C^{Li7}} \right) e^{-\bar{b}x} \quad (A6)$$

$$\frac{\partial C^{Li7}}{\partial t} = \frac{\partial^2 C^{Li7}}{\partial x^2} - \bar{A} \left(C^{Li7} + \frac{C_0^{Li7}}{\Delta C^{Li7}} \right) e^{-\bar{b}x} \quad (A7)$$

Here, $\bar{A} \equiv AL^2/D^{Li7}$ and $\bar{b} \equiv bL$ are the nondimensional extraction strength and the nondimensional decaying constant, respectively.

This problem was solved using a coordinate system with its origin set at the boundary between the dunite and the harzburgite units. The boundary conditions are that at $x = -L$, $C^{Li7} = C_0^{Li7}$ and $C^{Li6} = C_0^{Li6} = C_0^{Li7}/12.1163$. As $x \rightarrow \infty$, $C^{Li7} = C_{low}^{Li7}$ and $C^{Li6} = C_{low}^{Li6} = C_{low}^{Li7}/12.1163$. Notice also that $\Delta C^{Li7} = C_0^{Li7} - C_{low}^{Li7}$. The initial conditions are two step functions such that at $t = 0$, $C^{Li7} = C_0^{Li7}$ and $C^{Li6} = C_0^{Li6}$ for all x in the dunite, and $C^{Li7} = C_{low}^{Li7}$ and $C^{Li6} = C_{low}^{Li6}$ in the harzburgite.

To seek numerical solutions for the governing equations, the harzburgite is chosen to be 12.5 times as wide as the dunite unit. Although the choice of this distance is arbitrary, it turns out that such a distance is sufficiently far away that isotopic concentrations are not affected significantly over the time span of our model computation. The x increment is chosen to be 0.1, which implies a physical distance of one-tenth of the half-width of the dunite unit. For numerical stability, the time step of the computation must obey the following relationship (e.g., Smith, 1978):

$$\Delta t < \frac{1}{\frac{2}{\Delta x^2} + (\bar{A}e^{-\bar{b}x})_{\max}} \quad (A8)$$

All numerical solutions were calculated with a Sun Sparc workstation.